

An appetizer to modern developments on the Kardar-Parisi-Zhang universality class

Kazumasa A. Takeuchi

*Department of Physics, Tokyo Institute of Technology,
2-12-1 Ookayama, Meguro-ku, Tokyo 152-8551, Japan.*

Abstract

The Kardar-Parisi-Zhang (KPZ) universality class describes a broad range of non-equilibrium fluctuations, including those of growing interfaces, directed polymers and particle transport, to name but a few. Since the year 2000, our understanding of the one-dimensional KPZ class has been completely renewed by mathematical physics approaches based on exact solutions. Mathematical physics has played a central role since then, leading to a myriad of new developments, but their implications are clearly not limited to mathematics – as a matter of fact, it can also be studied experimentally. The aim of these lecture notes is to provide an introduction to the field that is accessible to non-specialists, reviewing basic properties of the KPZ class and highlighting main physical outcomes of mathematical developments since the year 2000. It is written in a brief and self-contained manner, with emphasis put on physical intuitions and implications, while only a small (and mostly not the latest) fraction of mathematical developments could be covered. Liquid-crystal experiments by the author and coworkers are also reviewed.

Keywords: Kardar-Parisi-Zhang universality class, interface growth, exact solution, Tracy-Widom distribution, random matrix theory, integrable system, exclusion process

1. Introduction

Physics of critical phenomena, as represented by those of the Ising model, is one of the monuments of statistical physics. From the author's possibly biased view, it was founded cooperatively by theoretical studies [1], both rigorous and non-rigorous, as well as by experiments [2]. More precisely, when Andrews discovered the liquid-vapor critical point in the 19th century [3], what he observed was the Ising critical behavior from the modern viewpoint, though the Ising model was invented much later. In the mid 20th century, the two-dimensional Ising model was solved exactly by Onsager, and subsequently by Kaufman and Nambu [4–7]. This exact solution clearly indicated the existence of nontrivial critical behavior that is different from the prediction of the mean field theory. Then it turned out that critical phenomena exhibit certain extent of universality, as suggested by experimental observations of liquid-vapor systems, binary liquid mixtures and magnets [2]. This universality was clearly accounted for by Wilson's renormalization group [8] on the basis of continuum equations such as the ϕ^4 model, which allowed us to classify critical phenomena in terms of universality classes. This line of research marked further milestones, such as the foundation of conformal field theory [9], and it continues doing so, as exemplified by recent developments of conformal bootstrap theory [10] tackling the three-dimensional Ising problem.

All these developments concern critical phenomena at thermal equilibrium. Then, does there exist such a beautiful physics for systems driven out of equilibrium? No one knows the answer yet, but developments that might resemble the dawn of the equilibrium counterpart can be found in recent studies on the Kardar-Parisi-Zhang (KPZ) universality class [11–17]. The KPZ class, best known as the simplest generic class for fluctuations of growing interfaces [11], is also related to a wide variety of non-equilibrium fluctuations, including directed polymers, stirred fluids, and particle transport to name but a few. Furthermore, for the one-dimensional (1D) case, mathematical studies have unveiled nontrivial connections to random matrix theory, combinatorial problems, and integrable systems. This has driven intense activities to investigate exact fluctuation properties of the 1D KPZ class and its mathematical structure behind, providing a great number of exact results [14–18] which also have experimental relevance [19–21].

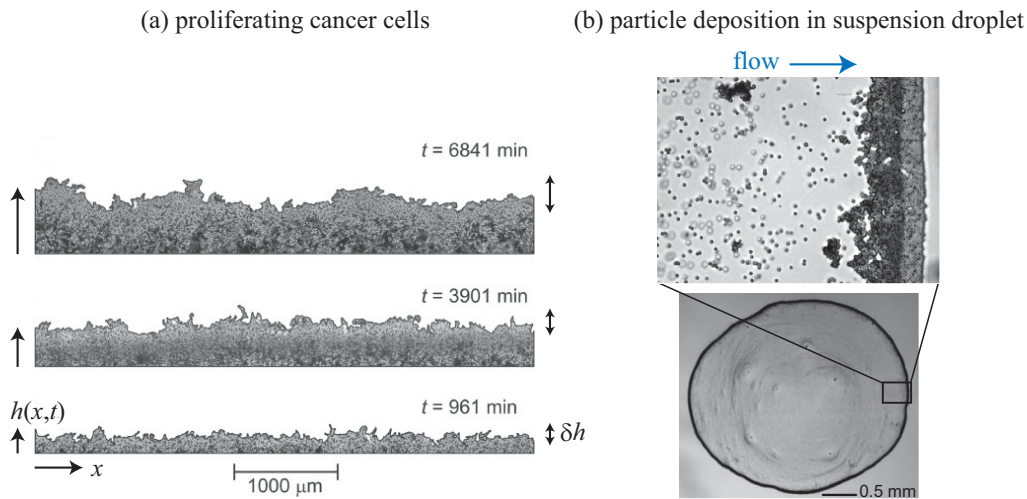


Figure 1: Experimental examples of growing interfaces. (a) Front evolution of cancer cell colonies (“HeLa cells” from human cervix cancer) cultured in Petri dishes [24]. Here the colonies are two-dimensional, so that the interfaces are one-dimensional, and they grow because of the division of cancer cells. The 1D KPZ exponents were found [24]. Similar growth was also observed with Vero cells (from African Green Monkey kidney), which are not tumorigenic but invasive [25, 26]. (b) Deposition of spherical colloid particles onto the edge of a suspension droplet, during its evaporation process [27]. Fluid flows outward because of capillary effect, carrying colloids and leaving them at the droplet edge. The 1D KPZ exponents were observed when slightly elongated particles were used [28]. Reprints with permission from [24](a) and [27](b) with some adaptations. The axes and the arrows, as well as the associated labels, are added by the present author. The displayed amplitudes of δh are only schematic.

The aim of these lecture notes is to tempt non-specialists into this rapidly evolving field around the KPZ class. It is *not* a review of recent mathematical approaches nor a technical guide to solve the problems, for which the readers are referred to more appropriate reviews [14, 15, 17, 18] and references therein. Instead, it is intended to provide useful information for non-specialist physicists to join the game, in a brief but self-contained manner: how the KPZ class is linked to various problems, what the main outcomes and implications for physicists are, and what kind of intuitions we can use, from the limited view of an experimentalist admirer and user of those mathematical developments.

These lecture notes are organized as follows. Section 2 describes what kind of interfaces we deal with, on the basis of some experimental observations. Section 3 introduces continuum equations and their associated universality classes, including the KPZ equation and the KPZ class, and review their basic properties. Properties of the KPZ equation are further described in Sec. 4. Sections 5 and 6 illustrate some exact results for the 1D KPZ class, focusing on the distribution of interface fluctuations. Section 7 reviews experimental observations of growing interfaces in turbulent liquid crystal, to be compared with the exact results described in the preceding sections. In Sec. 8 we briefly discuss the situation in higher dimensions. Section 9 provides brief concluding remarks.

2. Examples of quiescent and growing interfaces

The surface of water at rest is probably a symbol of something flat and smooth. Indeed, according to the capillary wave theory [22], which accounts for thermal excitations of such a free interface between two fluid phases, the amplitude of fluctuations under gravity is in the order of $\sqrt{k_B T / \gamma}$ with the Boltzmann constant k_B , temperature T , and interfacial tension γ . For molecular fluids, it is usually shorter than 1 nm [22, 23]; therefore, the interface is sufficiently smooth when observed at macroscopic length scales. But what happens if one of the phases is more stable than the other, hence taking over the region of the metastable state? What happens if one of the phases is solid and molecules are deposited on it one after another, such as in thin film growth? What happens if there is an aggregate of particles that can replicate themselves, such as living cells? Or, conversely, what happens if particles are being removed from the surface of the aggregate? In all such cases the interface (or the edge of the aggregate) would move in either direction, typically with fluctuations growing in time.

Let’s see some examples. Figure 1(a) shows snapshots of colonies of human cancer cells (HeLa), cultured in

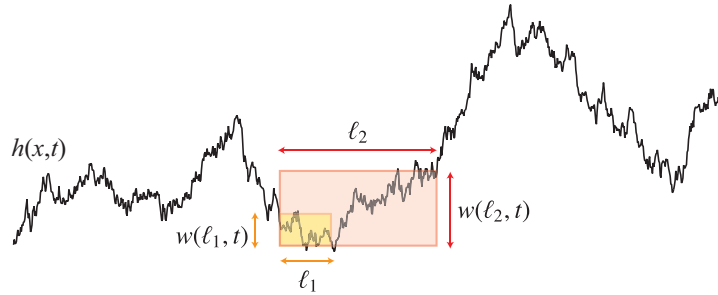


Figure 2: Sketch of the definition of the interface width $w(\ell, t)$. The standard deviation of $h(x, t)$ is calculated within a window of lateral size ℓ . It is then averaged over space (by shifting the window) and realizations, and this defines the interface width $w(\ell, t)$.

Petri dishes [24]. Those cells were initially cultured with an obstacle attached on the Petri dish bottom, which set the initially straight border of colonies. When the obstacle was removed, the colony starts to expand because of cell division and motility. As a result, the interface moves in the normal direction, but fluctuations also start to develop, because of the stochastic nature of cell behavior. Then the snapshots in Fig. 1(a) suggest that those interface fluctuations gain larger and larger structure as time elapses.

Figure 1(b) shows another example, taken from an experiment of “coffee ring effect” [27] – a familiar phenomenon observed when a droplet of coffee is dried on a solid surface, which leaves a ring of coffee particles on the surface. The formation of the ring is due to the deposition of particles onto the droplet edge, carried by fluid capillary flow. In Fig. 1(b), polystyrene beads were used as particles, and the deposition was monitored by a microscope (see also Supplementary Movie 3 of [27]). One can again see that, as the front of the deposited particles moves inward, its fluctuations develop, because of random deposition of particles. Here we can also see that those particles interact; sometimes they collide and stick to each other, and in fact they can interact through deformation of the air-liquid surface.

In the literature, such kinetic roughening of interfaces has been reported in a wide variety of growth processes [12, 13, 29], classical examples being bacteria colonies on agar, slow combustion of paper, growth of solid thin film, etc. Kinetic roughening seems to be a common feature of interfaces that grow through short-ranged interactions under the influence of noise, whether it is inherent to dynamics (such as cell division) or results from heterogeneity of the system (such as fibrous structure of paper)¹. Those interfaces are not merely similar in the qualitative sense, but in many cases they have a striking quantitative property, namely, scale invariance. The example of cancer cell colony growth in Fig. 1(a) beautifully shows that, as time t is increased, both the amplitude of interface fluctuations δh and the length of correlation in the spanwise direction x seem to grow. To quantify this, we define the height of interface $h(x, t)$ as a single-valued function of spanwise position x and time t (Fig. 1(a))² and measure the standard deviation of $h(x, t)$ within windows of lateral size ℓ , which is called the interface width $w(\ell, t)$ (Fig. 2). In many experiments, as well as in toy models of growth processes, the following power law has been found for this $w(\ell, t)$ [12, 13], called the

¹ In the presence of non-local interactions, kinetics and resulting morphology of interfaces can be very different. For example, if particles can diffuse freely in the surrounding environment before they adhere to the interface, the growth is controlled by the density field of diffusing particles, which is affected by the global structure of the interface. Fractals tend to appear in such a case; see [12].

² By using the single-valued function $h(x, t)$, we ignore overhangs of the interfaces. In the literature, a growth equation for an interface of general shape, including overhangs, was proposed [30]. On the basis of numerical results presented in that paper [30], the effect of overhangs seems to be minor. A few later numerical studies [31, 32] also reached the conclusion that overhangs do not seem to change the scaling laws of growing interfaces that we are interested in here. The use of the single-valued height $h(x, t)$ can be justified by these observations, and is also favored for the sake of simplicity. For those who analyze interface data, overhangs may simply be removed by taking, e.g., the maximum, the mean value, etc., of all the interface heights detected at each position x . Note, however, that there do exist other situations in which overhangs matter, especially if interfaces are pinned [33]. Therefore, from the experimental viewpoint, it may be worth trying analysis that takes account of overhangs, whenever they seem to have large-scale structure.

Family-Vicsek scaling³:

$$w(\ell, t) \sim t^\beta F_w(\ell t^{-1/z}) \sim \begin{cases} \ell^\alpha & \text{for } \ell \ll \xi(t), \\ t^\beta & \text{for } \ell \gg \xi(t), \end{cases} \quad \text{with } \xi(t) \sim t^{1/z} \quad (z \equiv \alpha/\beta), \quad (1)$$

and a scaling function $F_w(\cdot)$. This implies that the statistical properties of $\delta h(x, t) \equiv h(x, t) - \langle h(x, t) \rangle$ are kept invariant under the following scale transformation:

$$x \mapsto bx, \quad t \mapsto b^z t, \quad \delta h \mapsto b^\alpha \delta h. \quad (2)$$

Therefore, the set of the exponents α, β, z characterizes kinetic roughening, playing the role equivalent to the critical exponents of phase transitions. One may then expect that kinetic roughening can also be classified in terms of universality classes, which share the same values of the scaling exponents α, β, z . This is indeed the case, at least theoretically⁴, so that several universality classes and corresponding continuum equations have been proposed in the literature [12].

3. Continuum equations and universality classes

3.1. Edwards-Wilkinson equation

Now we attempt to construct, on the phenomenological basis, a continuum equation for the interface height $h(\mathbf{x}, t)$ growing on a d -dimensional substrate, i.e., $\mathbf{x} \in \mathbb{R}^d$ and $h, t \in \mathbb{R}$. The symmetry we expect for kinetic roughening is (i) invariance under time translation $t \mapsto t + t_0$, (ii) invariance under space translation $\mathbf{x} \mapsto \mathbf{x} + \mathbf{x}_0$, (iii) invariance under space inversion and rotation, e.g., $\mathbf{x} \mapsto -\mathbf{x}$, and (iv) invariance under height translation $h \mapsto h + h_0$. The possibly simplest such equation is the following linear partial differential equation, called the Edwards-Wilkinson (EW) equation:

$$\frac{\partial}{\partial t} h(\mathbf{x}, t) = v_0 + \nu \nabla^2 h + \eta(\mathbf{x}, t). \quad (3)$$

Here, $\eta(\mathbf{x}, t)$ is white Gaussian noise such that

$$\langle \eta(\mathbf{x}, t) \rangle = 0, \quad \langle \eta(\mathbf{x}, t) \eta(\mathbf{x}', t') \rangle = D \delta(\mathbf{x} - \mathbf{x}') \delta(t - t') \quad (4)$$

with ensemble average $\langle \cdot \rangle$, and v_0, ν, D are constant parameters. The second term of Eq. (3) corresponds to surface tension, or diffusion, which tends to smooth irregularities of the interface. The first term is simply a constant driving force. Since this term can be trivially removed by Galilean transformation $h \mapsto h + v_0 t$, i.e., by using the comoving frame, it is often omitted in the theoretical literature. As a result, the EW equation has an additional height inversion symmetry, i.e., (v) invariance under $h \mapsto -h$, in addition to the symmetries (i)-(iv) listed above.

To obtain the scaling exponents α, β, z for the EW equation, we may impose the invariance under the scale transformation (2) directly upon Eq. (3) with $h(x, t) = v_0 t + \delta h(x, t)$. This leads to $b^{\alpha-z} = b^{\alpha-2} = b^{-(d+z)/2}$, hence

$$\alpha = \frac{2-d}{2}, \quad \beta = \frac{2-d}{4}, \quad z = 2. \quad (\text{EW class}) \quad (5)$$

Although such naive power counting does not always work in general, for the EW equation it gives the correct exponent values, as one can easily check by solving Eq. (3) in Fourier space [12, 13].

Instead of directly solving for the height function $h(x, t)$, one can also deal with the probability density of the height profile $h(\mathbf{x})$ at time t , $P[h(\mathbf{x}), t]$, via the Fokker-Planck equation [34]. For the EW equation (3) with $v_0 = 0$, it

³ Alternatively, one can also use the height-difference correlation function $C_h(\ell, t) \equiv \langle [h(x + \ell, t) - h(x, t)]^2 \rangle$, which scales in the same way as $w(\ell, t)^2$ (with a different scaling function).

⁴ Unfortunately, universality is not as clear in experimental studies [12, 13], possibly because of some complexities in experimental systems and/or often limited length and time scales of observation, as well as limited statistical accuracy. However, recently, a growing number of experiments have shown exponent values in agreement with known universality classes, in particular the KPZ class [29]. The cancer colony growth [24] and the particle deposition [28] illustrated in Fig. 1 are among such experiments.

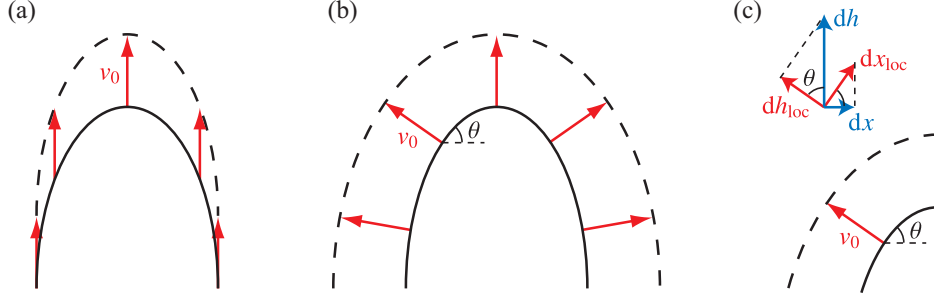


Figure 3: Sketch of the interface that grows according to the EW equation (a) and that grows in the locally normal direction (b). The effect of noise and diffusion is neglected in this sketch. The panel (c) illustrates how to transform the local coordinates $(h_{\text{loc}}, x_{\text{loc}})$ to the global ones (h, x) . This sketch is adapted from Fig. 3.1 in [13].

reads⁵

$$\frac{\partial}{\partial t} P[h(\mathbf{x}), t] = - \int d^d \mathbf{x} \frac{\delta}{\delta h} (v \nabla^2 h) P[h(\mathbf{x}), t] + \frac{D}{2} \int d^d \mathbf{x} \frac{\delta^2}{\delta^2 h} P[h(\mathbf{x}), t] \quad (6)$$

with the functional derivative $\frac{\delta}{\delta h}$, which formally corresponds to $\frac{\delta}{\delta h} = \frac{\partial}{\partial h} - \nabla \cdot \frac{\partial}{\partial (\nabla h)}$. Then the stationary solution to Eq. (6), $P_{\text{stat}}[h(\mathbf{x})]$, can be readily found to be

$$P_{\text{stat}}[h(\mathbf{x})] \propto \exp \left[- \int d^d \mathbf{x} \frac{v}{D} (\nabla h)^2 \right]. \quad (7)$$

In particular, for $d = 1$, it is *exactly* the probability density of the Brownian motion with diffusion coefficient $D/4v$, if x and h for the interface are interpreted as time and position, respectively, of the Brownian motion. In other words, if $B(t)$ denotes the Brownian motion with mean squared displacement $\langle [B(t) - B(0)]^2 \rangle = t$ (Wiener process [34]),

$$h_{\text{stat,1D}}(x) = \sqrt{AB}(x) \quad (A \equiv D/2v) \quad (8)$$

gives the statistically stationary solution of the 1D EW equation. Since $\langle [h_{\text{stat,1D}}(x + \ell) - h_{\text{stat,1D}}(x)]^2 \rangle \propto \ell$, this directly accounts for $\alpha = 1/2$ of the 1D EW class (see footnote 3).

3.2. Kardar-Parisi-Zhang equation

Since the EW equation is linear, many of its fluctuation properties can be solved exactly. But for this very reason, the EW equation is not sufficiently generic; growth processes in nature are in fact usually nonlinear. A simple geometric argument is enough to illustrate why growth is nonlinear in many cases.

Let's start from the EW equation (3). When we wrote it down, we had fixed the axes and implicitly assumed that the interface would always grow along the h -axis. This implies that, even a protrusion of the interface (Fig. 3(a)) would attempt to advance upward at speed v_0 , even though it will also be deformed by noise and diffusion of the EW equation. However, what happens more naturally is that the interface grows isotropically, so that each local piece of the interface advances in the direction normal to the interface (Fig. 3(b)). To take this effect into account, we may assume that the interface is evolved locally by the EW equation, with the height and space coordinates $(h_{\text{loc}}, x_{\text{loc}})$ taken locally

⁵ The functional version of the Fokker-Planck equation can be derived as follows. Consider the Langevin equation for multiple particles $X_i(t)$,

$$\frac{\partial X_i}{\partial t} = F_i[\{X_j\}] + \eta_i(t),$$

where $\{X_j\}$ denotes the all-particle configuration and $\eta_i(t)$ is white Gaussian noise with $\langle \eta_i(t) \rangle = 0$ and $\langle \eta_i(t) \eta_j(t') \rangle = D \delta_{ij} \delta(t - t')$. The corresponding Fokker-Planck equation is [34]

$$\frac{\partial}{\partial t} P[\{X_j\}, t] = - \sum_i \frac{\partial}{\partial X_i} F_i[\{X_j\}] P[\{X_j\}, t] + \frac{D}{2} \sum_i \frac{\partial^2}{\partial X_i^2} P[\{X_j\}, t].$$

Now, if we define $X_i \equiv h(x_i)$ with $x_i = i\Delta x$ and take the continuum limit $\Delta x \rightarrow 0$, we obtain the desired equation.

along the normal and tangential axes, respectively. Then we transform $(h_{\text{loc}}, x_{\text{loc}})$ to the global coordinates (h, x) and obtain a new equation. In order for the new coordinates to describe the desired interface evolution, their infinitesimal changes dh and dx should be associated with dh_{loc} and dx_{loc} in the following manner (Fig. 3(c)):

$$dh = dh_{\text{loc}} / \cos \theta = dh_{\text{loc}} \sqrt{1 + (\nabla h)^2}, \quad dx = dx_{\text{loc}} \cos \theta = dx_{\text{loc}} / \sqrt{1 + (\nabla h)^2}, \quad (9)$$

where θ is the local inclination angle, hence $\tan \theta = |\nabla h|$. By inserting it to the evolution of $(h_{\text{loc}}, x_{\text{loc}})$, i.e., the EW equation (3), and keeping only the lowest-order nonlinearity for small $|\nabla h|$, we obtain

$$\frac{\partial}{\partial t} h(\mathbf{x}, t) = v_0 + \nu \nabla^2 h + \frac{\lambda}{2} (\nabla h)^2 + \eta(\mathbf{x}, t), \quad (10)$$

where the noise $\eta(\mathbf{x}, t)$ is still given by Eq. (4). This is the KPZ equation, the (main) protagonist of these lecture notes. Note that the effect of the local slope discussed here is only one possible source of nonlinearity; in general there can be others, such as nonlinearity in interactions between constituent particles. Most probably, they also contribute to the $(\nabla h)^2$ term, which is indeed the lowest-order nonlinearity allowed by the symmetry requirements (i)-(iv) discussed in the previous section. Therefore, the KPZ equation is not necessarily a model of isotropic interfaces, but is a more generic model of interfaces growing under some nonlinear mechanisms. The coefficient λ of the $(\nabla h)^2$ term should be regarded as an independent parameter of the equation.

Some remarks are now in order. First, the constant term v_0 can still be got rid of by the Galilean transformation, so that we can set $v_0 = 0$ without loss of generality. Second, the nonlinear term $(\nabla h)^2$ breaks the height inversion symmetry (v) that the EW equation possesses. In this sense, the KPZ equation describes a *bona fide* growth process, which is not simply due to the constant term v_0 that can be removed. Finally, the newly added nonlinear term is relevant in the renormalization group sense [11–13], at least for the physically relevant dimensionalities $d \leq 2$. The KPZ equation therefore represents a new universality class, the KPZ class. For 1D, the values of the scaling exponents can be determined exactly to be

$$\alpha = 1/2, \quad \beta = 1/3, \quad z = 3/2 \quad (\text{1D KPZ class}) \quad (11)$$

because of certain symmetries that will be described in Section 4. In contrast, no exact values are known for higher dimensions; for $d = 2$, a recent numerical estimation [35] gave $\alpha = 0.3869(4)$, where the number in the parentheses indicates the uncertainty, from which $\beta = 0.2398(3)$ and $z = 1.6131(4)$ follow (using Eq. (18) explained below)⁶. Note that the naive power counting we did for the EW equation does not work here, because in general coefficients such as ν, λ, D can also change by the scale transformation (2). For the KPZ equation, dynamic renormalization group calculation [11–13] indeed shows that ν and D change with scale, while λ is actually scale-invariant. We will come back to this point in Section 4.1.

3.3. Mullins-Herring equation and its nonlinear variant

In the literature, there have been proposed a few other continuum equations and associated universality classes for kinetic roughening of interfaces. For example, if deposited particles have enough time to diffuse on the surface until the next particle is deposited, one obtains the following Mullins-Herring equation within the linear theory [12]:

$$\frac{\partial}{\partial t} h(\mathbf{x}, t) = v_0 - K \nabla^4 h + \eta(\mathbf{x}, t). \quad (12)$$

The nonlinear variant of this model reads

$$\frac{\partial}{\partial t} h(\mathbf{x}, t) = v_0 - K \nabla^4 h + \lambda_1 \nabla^2 (\nabla h)^2 + \lambda_2 \nabla \cdot (\nabla h)^3 + \eta(\mathbf{x}, t), \quad (13)$$

where the second nonlinear term $\lambda_2 \nabla \cdot (\nabla h)^3$ is often neglected, because its physical origin is unclear [12]. The corresponding universality classes are sometimes called the linear (Eq. (12)) and nonlinear (Eq. (13)) molecular beam epitaxy classes. The interested readers are referred to other reviews and textbooks, such as [12].

⁶ Note however that estimates from different studies still vary a little. See Table I in [35] as well as more recent work [36].

3.4. Growth under quenched noise and the quenched KPZ equation

For some experimental examples of growing interfaces, such as wetting fronts of paper [12], noise comes from heterogeneity of the medium. Then it may be more appropriate to replace the spatiotemporal noise $\eta(\mathbf{x}, t)$ that we have used in continuum equations by quenched noise $\eta_q(\mathbf{x}, h)$, which is now a function of \mathbf{x} and h and does not depend explicitly on time. If we do so for the KPZ equation, we obtain the quenched KPZ (qKPZ) equation:

$$\frac{\partial}{\partial t} h(\mathbf{x}, t) = F + v \nabla^2 h + \frac{\lambda}{2} (\nabla h)^2 + \eta_q(\mathbf{x}, h(\mathbf{x}, t)). \quad (14)$$

with

$$\langle \eta_q(\mathbf{x}, h) \eta_q(\mathbf{x}', h') \rangle = \delta(\mathbf{x} - \mathbf{x}') \Delta_\kappa(h - h'), \quad (15)$$

where $\Delta_\kappa(r)$ is an even function of r that monotonically decreases to zero over a finite distance κ (the delta correlation corresponds to $\kappa \rightarrow 0$)⁷. The constant term of Eq. (14) is denoted by F (for “force”) following the convention, which *cannot* be got rid of by Galilean transformation because of the explicit dependence of noise on h .

An important characteristic of the qKPZ equation is that it shows a pinning-depinning transition as the force F is varied. More specifically, if F is large enough, the interface will grow unceasingly. In this case $\eta_q(\mathbf{x}, h(\mathbf{x}, t))$ is equivalent to $\eta(\mathbf{x}, t)$, so that the interface is described by the KPZ scaling laws. In contrast, if F is small, there will be fractions of the interface that experience too strong negative noise $\eta_q(\mathbf{x}, h(\mathbf{x}, t))$ to be overcome by the given driving force F . Once they stop, they remain pinned, because the value of $\eta_q(\mathbf{x}, h(\mathbf{x}, t))$ does not change unless the interface moves. In this way, the interface will be entirely pinned eventually. Then, those pinning and depinning phases are separated by a critical force F_c . At $F = F_c$ the interface is governed by a distinct set of scaling laws. It is also seen if F is not exactly F_c , up to a crossover time, which can be longer than the finite observation time of experiments or simulations. Therefore, in practice, the scaling laws of critically pinned interfaces may appear in a region of parameter space.

In the literature, critically pinned interfaces have been studied with various models. The situation is rather involved and not fully understood; a few universality classes have been argued to arise in different situations (see [12, 33] and references therein). It seems to be important (but not only) whether or not overhangs are allowed and relevant, and whether or not nonlinearity is relevant at the critical point. Concerning the latter point, even among models with nonlinearity [corresponding to $\frac{\lambda}{2} (\nabla h)^2$ in Eq. (14)], for some models nonlinearity is relevant at the critical point, and for others it is not. More specifically, the coefficient λ was argued to behave as $\lambda \sim (F - F_c)^{-\phi}$ [12], so that it may diverge ($\phi > 0$) or vanish ($\phi < 0$) at the critical point. The directed percolation depinning model [12] is an example where overhangs are forbidden and nonlinearity is relevant, and is considered to represent the qKPZ universality class. In particular, for 1D, this model makes a connection to the critical behavior of the directed percolation universality class for absorbing-state phase transitions [37]. As a result, the scaling exponents of the 1D qKPZ class are given by $\alpha = \beta = \nu_\perp^{\text{DP}} / \nu_\parallel^{\text{DP}} \approx 0.633$ and $z = 1$ [12], where ν_\perp^{DP} and $\nu_\parallel^{\text{DP}}$ are the critical exponents for diverging correlation length and time of the directed percolation class, respectively. In contrast, if we set $\lambda = 0$ in Eq. (14), it is called the quenched Edwards-Wilkinson (qEW) equation, and the corresponding class is the qEW class. It is believed to describe the case in which both overhangs and nonlinearity are absent or irrelevant. If overhangs are allowed and relevant, the critical interface may become fractal and described by the ordinary isotropic percolation class in $(d + 1)$ spatial dimensions [33, 38, 39]. Some models, in particular the random field Ising model without spontaneous nucleation [12, 38], show a transition between the fractal and self-affine morphology (akin to qEW) for $d \geq 2$ (i.e., total spatial dimensionality ≥ 3) [12, 38, 39]. This transition is characterized by the tricritical percolation [39, 40].

4. Basic properties of the KPZ equation

In this section we concentrate on the KPZ equation (10) and study its basic properties. In the following, we set $v_0 = 0$ without loss of generality.

⁷ The delta correlation limit $\kappa \rightarrow 0$ is not taken here, because the critical force F_c of the pinning-depinning transition is known to diverge in this limit [12].

4.1. Relation to the noisy Burgers equation

Since the invention of the KPZ equation [11], its relation to a stirred fluid problem has been recognized⁸. To see this, take the gradient of the KPZ equation (10) and define $\mathbf{v}(\mathbf{x}, t) \equiv -\lambda \nabla h(\mathbf{x}, t)$, then we obtain

$$\frac{\partial \mathbf{v}}{\partial t} + (\mathbf{v} \cdot \nabla) \mathbf{v} = \nu \nabla^2 \mathbf{v} - \lambda \nabla \eta(\mathbf{x}, t). \quad (16)$$

It is the noisy Burgers equation, known as a simple theoretical model of randomly stirred fluid. As such, it satisfies a symmetry expected for fluid, namely the invariance under Galilean transformation, $\mathbf{v}(\mathbf{x}, t) \mapsto \mathbf{v}_0 + \mathbf{v}(\mathbf{x} - \mathbf{v}_0 t, t)$ with a constant vector \mathbf{v}_0 , for which we also use $\langle \eta(\mathbf{x}, t) \eta(\mathbf{x}', t') \rangle = \langle \eta(\mathbf{x} - \mathbf{v}_0 t, t) \eta(\mathbf{x}' - \mathbf{v}_0 t', t') \rangle = D \delta(\mathbf{x} - \mathbf{x}') \delta(t - t')$. In terms of the interface height $h(\mathbf{x}, t)$, this translates into the invariance under the following tilt transformation with any constant vector \mathbf{s} :

$$h_{\text{new}}(\mathbf{x}_{\text{new}}, t) = h(\mathbf{x}, t) + \mathbf{s} \cdot \mathbf{x} - \frac{\lambda}{2} \mathbf{s}^2 t, \quad \mathbf{x}_{\text{new}} = \mathbf{x} - \lambda \mathbf{s} t, \quad (17)$$

where the same averaging over noise is used. This is called the statistical tilt symmetry of the KPZ equation. Moreover, since the Galilean symmetry should remain unchanged under the scale transformation (2), we can conclude that the coefficient λ should be scale-invariant⁹. By applying the scale transformation (2) to the KPZ equation (10), this scale invariance of λ results in the following scaling relation,

$$\alpha + z = 2, \quad (18)$$

which is valid for the KPZ class in any dimension d .

4.2. Stationary probability density for the 1D KPZ equation and fluctuation-dissipation theorem

As we did for the EW equation, we can also write down the Fokker-Planck equation for the KPZ equation (10), which then reads:

$$\frac{\partial}{\partial t} P[h(\mathbf{x}), t] = - \int d^d \mathbf{x} \frac{\delta}{\delta h} \left[\nu \nabla^2 h + \frac{\lambda}{2} (\nabla h)^2 \right] P[h(\mathbf{x}), t] + \frac{D}{2} \int d^d \mathbf{x} \frac{\delta^2}{\delta^2 h} P[h(\mathbf{x}), t]. \quad (19)$$

Interestingly, for 1D (only), one can easily check that the stationary solution (7) for the EW equation, i.e., the probability density of the Brownian motion, is also the stationary solution for the KPZ equation¹⁰. This immediately gives $\alpha = 1/2$. Using the scaling relation (18) and $z \equiv \alpha/\beta$, we obtain $\beta = 1/3$ and $z = 3/2$, the complete set of the scaling exponents of the 1D KPZ class. The fact that the Brownian motion gives the stationary probability density of the 1D KPZ equation is actually a consequence of the fluctuation-dissipation theorem [42] that it satisfies. This implies that the field theory underlying the 1D KPZ equation is much simpler than its higher-dimensional counterparts [42].

4.3. Well-definedness of the KPZ equation and relation to the stochastic heat equation

After all the explanations given on the KPZ equation, it is, in fact, known to be ill-defined [17, 43, 44], even if we should decide not to care about mathematical subtleties. It is easy to see from the form of the KPZ equation (10), because, on the one side it has delta-correlated noise $\eta(\mathbf{x}, t)$, which is non-differentiable, and on the other side it asks to compute the squared gradient, $(\nabla h)^2$, which would diverge if the operation were carried out literally.

To circumvent this problem, we resort to the mapping to another stochastic process. Using the Cole-Hopf transformation

$$Z(\mathbf{x}, t) \equiv \exp \left[\frac{\lambda}{2\nu} h(\mathbf{x}, t) \right], \quad (20)$$

⁸ In fact, the basic scaling properties of the KPZ equation were studied before it was invented, in the context of the noisy Burgers equation [41].

⁹ To see this clearly, following [41], one may introduce a coefficient $\lambda_0 = 1$ to the advection term $(\mathbf{v} \cdot \nabla) \mathbf{v}$. Then the system is invariant under $\mathbf{v}(\mathbf{x}, t) \mapsto \mathbf{v}_0 + \mathbf{v}(\mathbf{x} - \lambda_0 \mathbf{v}_0 t, t)$, which physically corresponds to the Galilean transformation only if $\lambda_0 = 1$. This implies that λ_0 remains unity even after the scale transformation (2); in other words, λ_0 is scale-invariant. Now, if we define the velocity field anew by $\mathbf{v}'(\mathbf{x}, t) \equiv -\nabla h(\mathbf{x}, t)$, the noisy Burgers equation reads $\frac{\partial \mathbf{v}'}{\partial t} + \lambda (\mathbf{v}' \cdot \nabla) \mathbf{v}' = \nu \nabla^2 \mathbf{v}' - \nabla \eta(\mathbf{x}, t)$. As we have just learned, the coefficient of the advection term, which is now λ , is scale-invariant.

¹⁰ This is because $\int d\mathbf{x} \frac{\delta}{\delta h} (\nabla h)^2 P_{\text{stat}}[h(\mathbf{x}), t] = 0$ for 1D (but not otherwise).

we can *formally* rewrite the KPZ equation (10) to the following, stochastic heat equation:

$$\frac{\partial}{\partial t} Z(\mathbf{x}, t) = \nu \nabla^2 Z(\mathbf{x}, t) + \frac{\lambda}{2\nu} Z(\mathbf{x}, t) \text{ “}\times\text{” } \eta(\mathbf{x}, t), \quad (21)$$

where the meaning of “ \times ” will be explained soon. This equation can also be expressed as $dZ(\mathbf{x}, t) = \nu \nabla^2 Z(\mathbf{x}, t) dt + \frac{\lambda}{2\nu} Z(\mathbf{x}, t) \text{ “}\times\text{” } dB_\eta(\mathbf{x}, t)$ with $dB_\eta(\mathbf{x}, t) \equiv \eta(\mathbf{x}, t) dt$. Compared with the KPZ equation, the stochastic heat equation may look simpler because it is linear, but it is deceptively so, as we have the multiplicative noise term instead. According to stochastic calculus [34], whenever we have such multiplicative noise in a stochastic differential equation, we need to specify the definition of the product $Z(\mathbf{x}, t) \text{ “}\times\text{” } dB_\eta(\mathbf{x}, t)$. If we choose the Stratonovich product¹¹ $Z(\mathbf{x}, t) \circ dB_\eta(\mathbf{x}, t)$, the usual chain rule of differentiation can be used, so that the stochastic heat equation (21) is equivalent to the KPZ equation (10), but then both of them are ill-defined.

To see this clearly [17, 44], let’s consider the 1D case and replace the noise $\eta(x, t)$ by colored Gaussian noise $\eta_\kappa(x, t)$ such that

$$\langle \eta_\kappa(x, t) \rangle = 0, \quad \langle \eta_\kappa(x, t) \eta_\kappa(x', t') \rangle = D \Delta_\kappa(x - x') \delta(t - t'), \quad (22)$$

with

$$\Delta_\kappa(x) \equiv \frac{1}{\kappa \sqrt{\pi}} e^{-(x/\kappa)^2} \rightarrow \delta(x) \quad (\kappa \rightarrow 0). \quad (23)$$

Using the conversion formula between the Stratonovich and Itô products [34], we have

$$Z(x, t) \circ dB_{\eta_\kappa}(x, t) = Z(x, t) dB_{\eta_\kappa}(x, t) + \frac{1}{2} dZ(x, t) dB_{\eta_\kappa}(x, t), \quad (24)$$

where the products in the right hand side are now Itô’s ones. Then we obtain

$$\langle dZ(x, t) dB_{\eta_\kappa}(x, t) \rangle = \frac{\lambda}{2\nu} \langle Z(x, t) \rangle \langle dB_{\eta_\kappa}(x, t)^2 \rangle = \frac{\lambda}{2\nu} \langle Z(x, t) \rangle D \Delta_\kappa(0) dt = \frac{\lambda}{2\nu} \langle Z(x, t) \rangle \frac{D}{\kappa \sqrt{\pi}} dt, \quad (25)$$

which diverges in the limit $\kappa \rightarrow 0$. On the other hand, this singularity is not too pathologic because, if $\langle Z(x, t) \rangle$ is uniform in space, it simply amounts to uniform translation in h . It can therefore be removed by riding on the comoving frame, or, equivalently, using the Itô product from the beginning. Indeed, the stochastic heat equation with the Itô product

$$\frac{\partial}{\partial t} Z(x, t) = \nu \nabla^2 Z(x, t) + \frac{\lambda}{2\nu} Z(x, t) \eta(x, t), \quad (26)$$

can be shown to be mathematically well-defined, at least for 1D [17, 43–46]. Therefore, we can start from Eq. (26) and *define*

$$h(x, t) \equiv \frac{2\nu}{\lambda} \log Z(x, t). \quad (27)$$

Suppose a solution $Z(x, t)$ to Eq. (26) is obtained, $h(x, t)$ defined by Eq. (27) is formally called the “solution of the KPZ equation” in the literature¹².

5. Exact results on the 1D KPZ class 1: polynuclear growth model

From the beginning of its history, the KPZ class has been extensively studied as an instance of non-equilibrium scaling laws. However, it is since the year 2000 that our understanding of the KPZ class has been dramatically

¹¹ For the stochastic differential equation $dZ(t) = F(Z(t), t) dt + G(Z(t), t) \text{ “}\times\text{” } dB(t)$ with infinitesimal increment $dB(t) \equiv B(t + dt) - B(t)$ of the Wiener process $B(t)$, the Stratonovich product $G(Z(t), t) \circ dB(t)$ is defined as the continuum limit of $G(\frac{Z(t_{i+1}) + Z(t_i)}{2}, t_i) [B(t_{i+1}) - B(t_i)]$, and the Itô product $G(Z(t), t) dB(t)$ is the continuum limit of $G(Z(t_i), t_i) [B(t_{i+1}) - B(t_i)]$ [34]. While for the Stratonovich product we can use the usual chain rule of differentiation, the Itô product has a great advantage that the two operands $G(Z(t_i), t_i)$ and $B(t_{i+1}) - B(t_i)$ are stochastically independent.

¹² As an alternative approach, Hairer extended what is called the rough path theory in mathematics and successfully provided a mathematical foundation to the KPZ equation [47]. This approach was then further developed to the theory of regularity structures [48]. For this series of work, Hairer was awarded a Fields Medal of the year 2014.

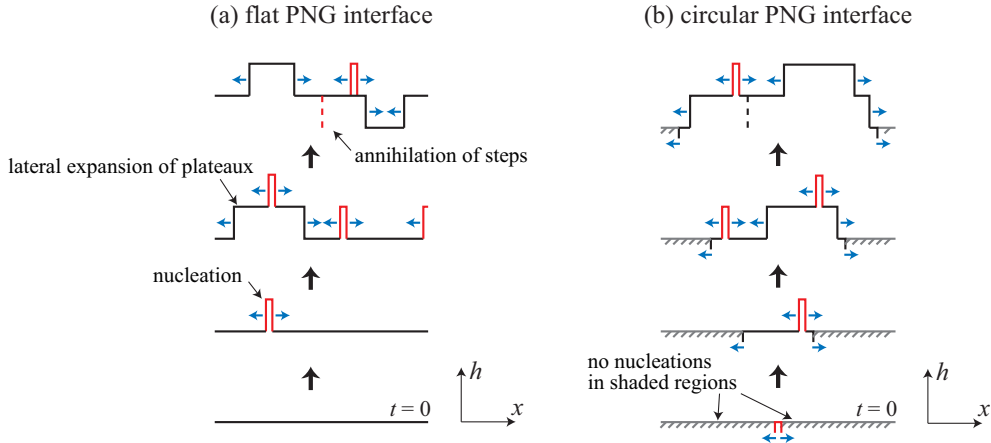


Figure 4: Sketch of a flat (a) and a circular (b) PNG interface. In the circular case (b), nucleations do not occur in the shaded regions, $|x| > t$.

changed, when a few models in the 1D KPZ class were solved with mathematical rigor for the first time [49, 50]. The first results were obtained on the one-point distribution of the height $h(x, t)$. The developments have soon extended to other statistical quantities, such as the correlation function in space, as well as to more generalized models in the 1D KPZ class. This led to further breakthroughs, in particular the establishment of exact solutions to the 1D KPZ equation proper since 2010 [44–46, 51–55]. These activities from mathematics and mathematical physics continue marking rapid progress [14–18]. While they are certainly interesting and important in their own, they have also conveyed a lot of physical implications, which non-specialists may overlook when reading mathematical literature. The aim of the present and following sections is, therefore, to illustrate some important rigorous results with emphasis put on physical implications and intuitions, which allow the author to work in this field by experimental and numerical approaches.

In the present section, we concentrate on a model called the polynuclear growth (PNG) model, which is one of the first models that were solved exactly. By following Prähofer and Spohn’s celebrated paper [50], it will be illustrated how the model is related to a number of different problems, how the exact results were derived, and what the outcome is from the physics viewpoint. In particular, it will turn out that the KPZ class splits into at least a few *universality subclasses* as the author calls, for which the scaling exponents are the same (Eq. (11)) but nevertheless other statistical properties of the height fluctuations, in particular their distribution and correlation properties, are different.

5.1. Definition of the 1D PNG model

The PNG model is a discrete model in the KPZ class, which describes a growth process driven by random creations of nuclei (Fig. 4(a)). For 1D, $x, t \in \mathbb{R}$ and $h(x, t) \in \mathbb{Z}$. Starting from $h(x, 0) = 0$ (bottom sketch of Fig. 4(a)), there is a probability ρ over unit space and unit time that a point nucleus is generated (second sketch). If this happens at position x_n and time t_n , the height $h(x_n, t_n)$ is incremented by one, i.e., $h(x_n, t_n) \mapsto h(x_n, t_n) + 1$. Then the steps at both ends of the nucleus separate laterally, each at constant speed v (third sketch). When two steps from different nuclei meet each other, they simply annihilate (top sketch). These ingredients (except the random nucleation) can be expressed by a single equation, $h(x, t + dt) = \max_{x-vdt \leq x' \leq x+vd t} h(x', t)$. Nucleations can also occur on top of the expanding plateaux. As a result, the PNG model, without any constraint, produces an on average flat interface that grows upward. In the following, we set $\rho = 1$ and $v = 1$ without loss of generality. Note that we consider an infinitely large system, so that we do not need to set the boundary condition.

5.2. PNG circular interface

While the flat case depicted in Fig. 4(a) is simplest in view of the definition of the model, its variant for curved interfaces actually corresponds to the most fundamental case for our purpose. To deal with a curved interface in the PNG model, one can impose a constraint that nucleations can occur only within the region $|x| \leq t$ (see Fig. 4(b)). Then the generated interface is bounded by the two extremities that are fixed at $h(\pm t, t) = 0$, hence it is curved.

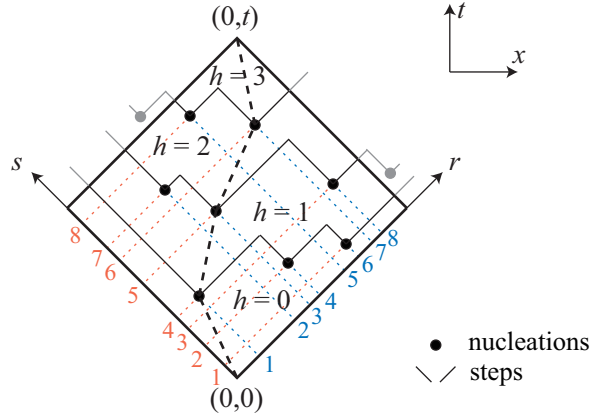


Figure 5: An example of the space-time plot for the circular PNG problem. This sketch is adapted from Fig. 1 in [50].

To describe the evolution of such a curved interface, it is useful to make a space-time plot showing where and when the nucleations occur, and along which paths their steps propagate. Figure 5 shows an example of such a space-time plot. In this plot, nucleations (black and gray dots) are generated randomly and independently at density $\rho = 1$ per unit area (Poisson point process), above the diagonal base lines that are depicted as the axes r and s . Each nucleation then produces steps (black and gray solid thin lines) that propagate diagonally. When two diagonal lines meet, they terminate.

Now our quantity of interest is the height $h(0, t)$ at position $x = 0$ and time t . First of all, because the “speed of light” of this PNG model is $v = 1$, it is sufficient to consider only the square region enclosed by bold black lines in Fig. 5. Next, we notice that the paths of the plateau steps (black thin lines) are the boundaries of the space-time regions with different heights. In other words, the height $h(x, t)$ increases by one each time we cross a black thin line. Therefore,

$$h(0, t) = \# \text{ of black thin lines to cross when moving from point } (0, 0) \text{ to point } (0, t), \quad (28)$$

under the constraint that the trajectory is always oriented upward, or more precisely, within the angle 45° to 135° . Within the same constraint, it is also

$$(28) = \text{maximal \# of black dots passed by a string (=directed polymer) with end points fixed at } (0, 0) \text{ and } (0, t), \quad (29)$$

as shown by the bold dashed line in Fig. 5. In other words, it is the (sign-flipped) ground-state energy of this directed polymer under a random potential $U(x, t) = -\sum_n \delta(x - x_n)\delta(t - t_n)$. Now we write down coordinates of the black dots, i.e., nucleation points. Here the coordinates are simply defined as indices along the two diagonal axes r and s , as illustrated in Fig. 5. If we arrange the sets of the coordinates in ascending order along one of the two axes, say r , we obtain $r : (1\ 2\ 3\ 4\ 5\ 6\ 7\ 8)$ for the example of Fig. 5. This is precisely a random permutation, whose length is generated randomly according to the Poisson distribution of mean $\rho S = t^2/2$, where S is the area of interest (the square region). Then, selecting a set of black dots to pass amounts to extracting a subsequence of the random permutation, and the directedness of the polymer is equivalent to the monotonic increase of the subsequence. To sum up, together with Eqs. (28) and (29),

$$h(0, t) = \text{length of longest increasing subsequence of a random permutation} \\ \text{whose length is generated according to the Poisson distribution with mean } t^2/2. \quad (30)$$

This is called Ulam’s problem.

Now the problem is purely combinatorial. In fact, there had been important advances in combinatorics [56] that allowed one to explicitly compute this problem, by employing mathematical tools called the Young tableaux and the

Robinson-Schensted correspondence. The final result is surprisingly simple: for large t ,

$$h(0, t) \simeq 2\sqrt{S} + S^{1/6}\chi_2 = \sqrt{2}t + (t/\sqrt{2})^{1/3}\chi_2. \quad (31)$$

Here, the exponent $1/3$ confirms that this model is in the KPZ class, and χ_2 is a random number generated according to a certain distribution known from random matrix theory [57, 58], namely the GUE Tracy-Widom distribution [59] for the largest eigenvalue of GUE random matrices (see next subsection). Moreover, it is straightforward to extend this result for $h(x, t)$, as it simply amounts to considering a rectangular region in the space-time plot, set by points $(0, 0)$ and (x, t) . We can use the same formula (31) with $S = (t^2 - x^2)/2$. This also tells us that $\langle h(x, t) \rangle \simeq \sqrt{2(t^2 - x^2)}$; in other words, our interface has a semicircle mean profile.

The bottom line so far is that the one-point distribution of the height fluctuations is explicitly obtained, is not Gaussian, and has a nontrivial connection to random matrix theory. We have also seen that this model is related to a number of apparently different problems, such as directed polymer in random medium¹³ and Ulam's problem in combinatorics.

5.3. Random matrix theory

Since a relation to random matrix theory has been encountered in the previous subsection, here we study some of its notions and results that are relevant for our purpose.

Random matrix theory [57, 58] deals with fluctuation properties of eigenvalues of matrices made of random numbers. Among them, matrices of Gaussian random numbers constitute the most fundamental ensembles of random matrices. For example, an ensemble called the Gaussian unitary ensemble (GUE) considers a large complex Hermitian random matrix

$$M = \begin{pmatrix} M_{11} & M_{12} & \cdots & M_{1N} \\ M_{21} & M_{22} & \cdots & M_{2N} \\ \vdots & \vdots & \ddots & \vdots \\ M_{N1} & M_{N2} & \cdots & M_{NN} \end{pmatrix} \quad (32)$$

with

$$M_{ii} = a_{ii}, \quad M_{ij} = \bar{M}_{ji} = a_{ij} + ib_{ij} \quad (i < j), \quad (33)$$

where $a_{ii} \in \mathbb{R}$ is an independent and identically distributed (iid) Gaussian random number with mean 0 and variance $1/2$, and $a_{ij}, b_{ij} \in \mathbb{R}$ are iid Gaussian random numbers with mean 0 and variance $1/4$. This somewhat strange choice of the variances is made in order that the probability density of this matrix can be given by the following simple form¹⁴

$$P(M) = \frac{1}{Z} e^{-\frac{\beta}{2} \text{Tr} M^2}, \quad (34)$$

with $\beta \equiv 2$ and normalization constant Z . This probability density is defined in such a way that $P(M)dM$ with $dM \equiv \prod_{i=1}^N da_{ii} \prod_{i < j} da_{ij} db_{ij}$ gives the probability to find the matrix elements a_{ij}, b_{ij} in the range $[a_{ij}, a_{ij} + da_{ij}]$ and $[b_{ij}, b_{ij} + db_{ij}]$. Similarly, the Gaussian orthogonal ensemble (GOE) consists of real symmetric matrices, distributed according to Eq. (34) with $\beta = 1$, and the Gaussian symplectic ensemble (GSE) concerns quaternion self-dual Hermitian matrices with $\beta = 4$.

Now we are interested in the distribution of the eigenvalues of the matrix M , denoted by $\lambda_1, \lambda_2, \dots, \lambda_N$. By diagonalizing, we have

$$M = UXU^{-1}, \quad X = \begin{pmatrix} \lambda_1 & & 0 \\ & \ddots & \\ 0 & & \lambda_N \end{pmatrix}, \quad dM = J(U, X)dUdX, \quad (35)$$

¹³ Note, however, that the connection between KPZ and the directed polymer has been known for a long time [13], even from the beginning of the history [11].

¹⁴ It is an unfortunate conflict that the letter β is used both for the parameter of the random matrix ensembles and for the growth exponent of kinetic roughening, predominantly in both contexts. In these lecture notes, β is used as the random matrix parameter only in Sec. 5.3; otherwise it is used as the interface growth exponent.

where U is an orthogonal (GOE), unitary (GUE), or symplectic (GSE) matrix and $J(U, X)$ is the Jacobian for this transformation. By computing this Jacobian, one obtains the following probability density of the eigenvalues [57, 58]

$$P(\lambda_1, \dots, \lambda_N) = \frac{1}{Z} \prod_{i < j} |\lambda_i - \lambda_j|^\beta \prod_i e^{-\frac{\beta}{2} \lambda_i^2}, \quad (36)$$

where we redefined the normalization Z . This is equivalent to the canonical ensemble of particles λ_i interacting through the following Hamiltonian:

$$H = \sum_i \frac{1}{2} \lambda_i^2 - \sum_{i < j} \log |\lambda_i - \lambda_j|, \quad (37)$$

i.e., with a harmonic trap and logarithmic repulsions, under the inverse temperature β .

We are almost there; what we encountered in the previous subsection was the distribution of the largest eigenvalue λ_{\max} of GUE random matrices. By using Eq. (36), it is simply expressed by

$$\text{Prob}[\lambda_{\max} \leq x] = \text{Prob}[\lambda_1, \dots, \lambda_N \leq x] = \frac{1}{Z} \int_{(-\infty, x]^N} \prod_i d\lambda_i \prod_{i < j} |\lambda_i - \lambda_j|^\beta \prod_i e^{-\frac{\beta}{2} \lambda_i^2}. \quad (38)$$

For large N , it is known to scale as

$$\lambda_{\max} \simeq \sqrt{2N} + 2^{-1/2} N^{-1/6} \chi_{\text{TW}, \beta}. \quad (39)$$

The analytic expression for this $\chi_{\text{TW}, \beta}$ was explicitly obtained by Tracy and Widom [59, 60], hence its distribution is called the Tracy-Widom distribution¹⁵. For reference, in the case of GUE, it is

$$\text{Prob}[\chi_{\text{TW}, \beta=2} \leq x] \equiv F_2(x) = \det(1 - P_x K P_x), \quad (40)$$

where P_x is the projection onto $[x, \infty)$, $K(x, y)$ is the Airy kernel

$$K(x, y) \equiv \frac{\text{Ai}(x) \text{Ai}'(y) - \text{Ai}(y) \text{Ai}'(x)}{x - y} \quad (41)$$

with the Airy function $\text{Ai}(x)$, and \det is the Fredholm determinant [57, 58, 62], an extension of determinant for function space, defined by

$$\det(1 + zK) \equiv \sum_{n=0}^{\infty} \frac{z^n}{n!} \int_{(-\infty, \infty)^n} \det[K(x_i, x_j)_{i, j=1}^n] dx_1 \cdots dx_n. \quad (42)$$

This can be approximated in terms of the usual matrix determinant [62]. The GUE Tracy-Widom distribution can also be expressed as follows. Let $u(x)$ be the global positive solution of the Painlevé II equation [63]

$$\frac{d^2 u}{dx^2} = 2u(x)^3 + xu(x), \quad (43)$$

and define $g(x)$ such that $g''(x) = u(x)^2$ and $g(x) \rightarrow 0$ as $x \rightarrow \infty$. Then one simply has $F_2(x) = e^{-g(x)}$ [50, 59]. With the same $g(x)$, and $f(x)$ such that $f'(x) = -u(x)$ and $f(x) \rightarrow 0$ as $x \rightarrow \infty$, the GOE Tracy-Widom distribution $F_1(x) \equiv \text{Prob}[\chi_{\text{TW}, \beta=1} \leq x]$ is given by $F_1(x) = e^{-[f(x)+g(x)]/2}$ [50, 60].

Figure 6 shows the probability density of the Tracy-Widom distributions for GOE, GUE, and GSE random matrices. As we can see, they are skewed and off-centered distributions. Their left tail decays as $e^{-\frac{\beta}{24} |\chi_{\text{TW}, \beta}|^3}$ and right tail as $e^{-\frac{2\beta}{3} \chi_{\text{TW}, \beta}^{3/2}}$ [64]. The left tail decays faster because, in order for the largest eigenvalue to be smaller, it needs to push all the other eigenvalues to its left.

¹⁵ Now the Tracy-Widom distribution is popular enough so that the function `TracyWidomDistribution` was implemented in Mathematica version 11. Otherwise, a numerical table of the GUE and GOE Tracy-Widom distribution can be downloaded by courtesy of Prähofer and Spohn [61].

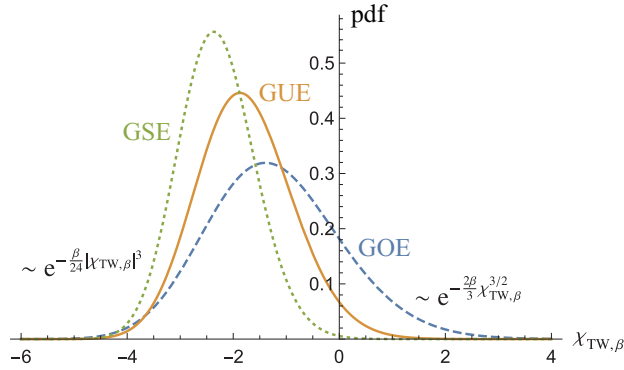


Figure 6: Tracy-Widom distribution for GOE (blue dashed line), GUE (orange solid line), and GSE (green dotted line) random matrices. These were drawn by Mathematica `TracyWidomDistribution` function.

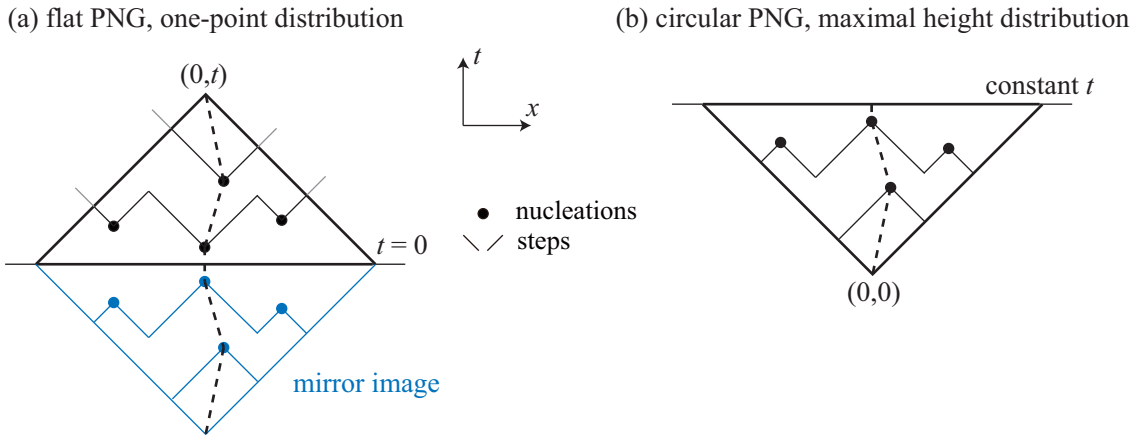


Figure 7: An example of the space-time plot for the one-point distribution of the flat PNG problem (a) and for the maximal height distribution of the circular PNG problem (b).

5.4. PNG flat interface

Now we come back to the exact results on the PNG model [50]. In Sec. 5.2, we dealt with the PNG circular interfaces and the GUE Tracy-Widom distribution appeared as the one-point distribution of the height function, i.e., $\chi_2 = \chi_{\text{TW},2}$ in Eq. (31). In the present subsection, we consider flat PNG interfaces (Fig. 4(a)), obtained from the initial condition $h(x, 0) = 0$ without any constraint on the nucleation region.

First we draw a space-time plot, similar to Fig. 5 we did for the circular case. In fact the only difference from the circular case is that now nucleations can occur anywhere on the substrate, so that the base line of the space-time plot is simply the horizontal line $t = 0$ (Fig. 7(a)) instead of the diagonal axes r and s for the circular case. In other words, the space-time region to consider is a triangle determined by the line $t = 0$ and the point $(0, t)$. In terms of the directed polymer, it is now a “point-to-line problem” (one fixed end and one free end), in contrast to the point-to-point problem (both ends fixed) for the circular case. Then, by putting the mirror image beneath the line $t = 0$, this triangular problem can be reduced to the squared problem we considered for the circular case, except that now we obviously have time-reversal symmetry in the nucleation points. This symmetry is translated to a reflection symmetry of the random permutation¹⁶, which is known to change the resulting distribution from the GUE Tracy-Widom to its GOE counterpart [65]. More specifically, since h and t in Fig. 5 should be now replaced by $2h$ and $2t$, respectively,

¹⁶ Suppose an integer index r (coordinate in Fig. 5) is permuted to $s = p(r)$, this reflection symmetry reads $p(N + 1 - p(r)) = N + 1 - r$, where N is the length of the permutation [50].

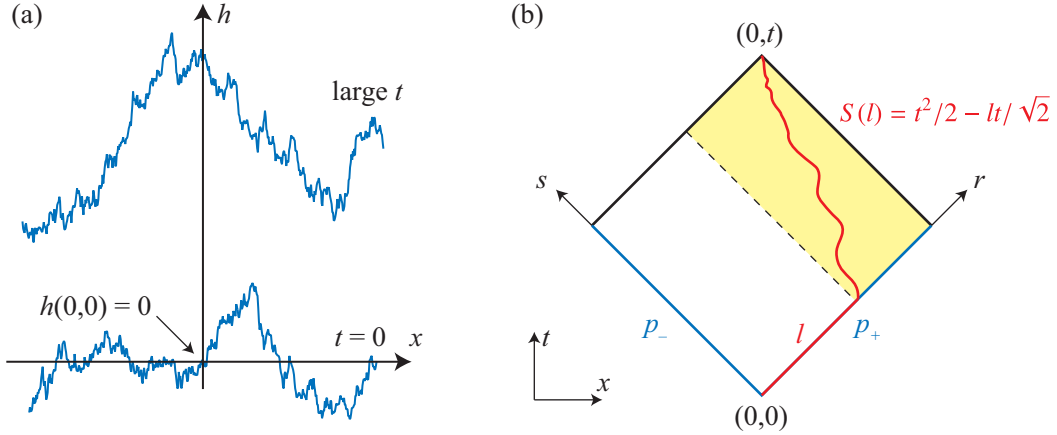


Figure 8: Stationary PNG problem. (a) Sketch of the stationary KPZ problem. (b) Space-time plot to consider for the stationary PNG problem. In addition to bulk nucleations at density ρ per unit area, one also has boundary nucleations on the r - and s -axis, at density p_+ and p_- , respectively, per unit length. As a result, the optimal path of the directed polymer (red bold line) can stay on the boundary for a finite length l and then wander in the bulk (yellow shaded area), whose remaining area is $S = t^2/2 - lt/\sqrt{2}$.

we obtain

$$\begin{aligned}
 2h(0, t) &\simeq \sqrt{2}(2t) + (2t/\sqrt{2})^{1/3} \chi_{\text{TW},1}, \\
 \therefore h(0, t) &\simeq \sqrt{2}t + (t/\sqrt{2})^{1/3} \chi_1 \quad \text{with } \chi_1 \equiv 2^{-2/3} \chi_{\text{TW},1}.
 \end{aligned} \tag{44}$$

Therefore, apart from the uninteresting factor $2^{-2/3}$, the one-point distribution of the flat PNG interfaces is the GOE Tracy-Widom distribution, instead of the GUE Tracy-Widom that appeared for the circular case. It is counterintuitive that fluctuation properties of the circular and flat interfaces are distinct even in the limit $t \rightarrow \infty$, because the mean profile of the circular interfaces becomes flatter and flatter as time goes on. Nevertheless, it is the truth, at least for the PNG model, as it is a rigorous result.

For physicists, we may argue that the presence or absence of the time-reversal symmetry in the PNG space-time plot is essential for having the different asymptotic properties of the flat and circular interfaces. This symmetry argument is indeed useful, because it helps to guess what we should obtain from the maximal height $\max_x h(x, t)$ of the circular PNG interfaces. Here, since the geometry is circular, we have the diagonal base lines in the space-time plot. But now, at time t , we scan all end points (x, t) with varying x to find the maximum of $h(x, t)$. This corresponds to the triangular space-time geometry as drawn in Fig. 7(b), which has the exactly same symmetry as for the one-point distribution in the flat case. We can therefore expect the GOE Tracy-Widom distribution for the maximal height of the circular interfaces, which was indeed shown to be true by both rigorous and non-rigorous approaches [66–68].

5.5. PNG stationary interface

Finally we aim to investigate the (statistically) stationary state of the PNG model. The question to ask is, if we take a stationary interface profile as the initial condition $h(x, 0)$ and set the origin at $h(0, 0) = 0$, what the distribution of $h(0, t)$ is for large t (Fig. 8(a)).

To deal with this stationary PNG problem, we first consider the following extension of the circular problem: in addition to bulk nucleations that occur in $|x| \leq t$ at rate $\rho = 1$, we have nucleations at the boundaries $x = \pm t$, i.e., on the r - and s -axes of the space-time plot (Fig. 8(b)). The boundary nucleations occur at rate p_+ and p_- on the r - and s -axes, respectively, per unit length of the space-time plot. Depending on the balance between the bulk and boundary nucleations, the directed polymer can stay on either boundary over some length, denoted by l , before jumping to the bulk. Once the polymer leaves the boundary, it cannot go back because of the directedness of the polymer. Then the height $h(0, t)$ can be decomposed into the bulk and boundary contributions, $h_{\text{bulk}}(l)$ and $h_{\pm}(l)$, respectively, as follows:

$$h = \max_{l, \pm} (h_{\text{bulk}}(l) + h_{\pm}(l)) \tag{45}$$

with

$$h_{\text{bulk}}(l) \simeq 2\sqrt{S} + S(l)^{1/6}\chi_2, \quad h_{\pm}(l) \simeq (p_{\pm}l) + (p_{\pm}l)^{1/2}\chi_G, \quad (46)$$

where $S(l) = t^2/2 - lt/\sqrt{2}$ is the remaining area of the bulk (yellow shaded area of Fig. 8(b)), the double sign indicates the choice of the boundary, and χ_G is a random variable drawn from the normal distribution (zero mean, unit variance). To determine the maximizer l , for large t , it is sufficient to consider the leading terms only, $F(l) \equiv 2\sqrt{S(l)} + p_{\pm}l$, then $F'(l_{\text{max}}) = 0$ with

$$l_{\text{max}} = \frac{t}{\sqrt{2}} \left(1 - \frac{1}{p_{\pm}^2}\right). \quad (47)$$

Therefore, if $p_{\pm} > 1$, the polymer stays on the boundary up to l_{max} . If $p_{\pm} < 1$, the polymer lives in the bulk only. $p_{\pm} = 1$ is critical. Assuming $p_+ \geq p_-$ without loss of generality, we can classify the situation as follows:

- $p_- \leq p_+ < 1$: bulk is dominant, $h(0, t)$ shows the GUE Tracy-Widom distribution.
- $p_+ > 1$ and $p_+ \neq p_-$: boundary is dominant (for the fluctuations), $h(0, t)$ shows the Gaussian distribution.
- $p_+ = p_- > 1$: boundary is dominant, $h(0, t)$ shows the (Gaussian)² distribution, i.e., the distribution of the maximum of two iid Gaussian variables.
- $p_+ = 1$ and $p_- < 1$: critical, the distribution is known to be the (GOE Tracy-Widom)² distribution [50, 69].
- $p_+ = p_- = 1$: critical, a new distribution was found for this case [50, 69], called the Baik-Rains distribution.

Now we want to relate this external source problem to the stationary state of the PNG model. Let $\rho_{\uparrow} = \rho_{\downarrow}$ be the density of upward and downward steps, respectively, in the stationary state (steps of plateaux in Fig. 4). In the stationary state, the step creation rate ρ must be balanced with the step annihilation rate, so that

$$\rho dx dt = (\rho_{\uparrow} dx)(\rho_{\downarrow} 2v dt). \quad (48)$$

Here the first factor of the right hand side indicates the probability to find an upward step in the range dx , and the second factor is the probability that it encounters a downward step within time interval dt . Then we obtain $\rho_{\uparrow}\rho_{\downarrow} = \rho/2v = 1/2$, hence $\rho_{\uparrow} = \rho_{\downarrow} = 1/\sqrt{2}$, which is the density of steps measured along the x axis. If the density is measured along the r - and s -axes, it is one, which coincides exactly with $p_+ = p_- = 1$ that gave the Baik-Rains distribution. Therefore, for the PNG stationary state,

$$h(0, t) \simeq \sqrt{2}t + (t/\sqrt{2})^{1/3}\chi_0, \quad (49)$$

with χ_0 being a random number drawn from the Baik-Rains distribution¹⁷.

To the author's knowledge, no connection between the Baik-Rains distribution and random matrix theory is known. However, using $f(x)$ and $g(x)$ associated with the Painlevé II equation (43), the Baik-Rains distribution can be expressed as [50, 69]

$$\text{Prob}[\chi_0 \leq x] \equiv F_0(x) = [1 - (x + 2f''(x) + 2g''(x))g'(x)] e^{-2f(x)-g(x)}. \quad (50)$$

5.6. Universality subclass

The results obtained in Secs. 5.2, 5.4, 5.5 prove that the one-point distribution of the PNG height fluctuations is different among the circular, flat, and stationary cases. In other words, the distribution changes according to the global geometry of the interfaces, i.e., whether the interface is circular, flat, or stationary (Brownian), or equivalently, depending on the initial condition¹⁸. On the other hand, we may still expect universality¹⁹; the same distribution may

¹⁷ Note that $h(0, 0) = 0$ by construction, while $h(x, 0)$ is not necessarily zero for $x \neq 0$. Therefore, for general x , one should measure the height difference in time, $h(x, t) - h(x, 0)$, to find the Baik-Rains distribution.

¹⁸ Instead of imposing the constraint on the nucleations in the circular PNG problem, one can equivalently use the following initial condition: $h(x, 0) = 0$ at $x = 0$ and $h(x, 0) = -\infty$ otherwise.

¹⁹ Universality is expected from the viewpoint of physics of critical phenomena. On the other hand, the exact derivation of the Tracy-Widom distributions relies on the integrability of the studied models, which is usually a fragile property. Therefore, at least to the author, it is not trivial whether the Tracy-Widom distributions and related statistical properties arise universally in the KPZ class, including non-integrable models and experimental systems.

arise for more general initial conditions, if they share the same symmetry (and other global properties), as well as for other systems in the KPZ class. Indeed, there is now overwhelming evidence that this geometry dependence is not a special property of the PNG model; instead, it is known to occur in various models [14–18] and in experiments [20, 21] as well. Moreover, this is not restricted to the one-point distribution either; while the scaling exponents α, β, z are left unchanged, many other statistical properties, in particular correlation properties, are known to change accordingly (see Sec. 6.3 for the spatial correlation). In view of this, it may be convenient to regard the three cases as different *universality subclasses*, within the single KPZ class. The different subclasses share the same scaling exponents, but are otherwise characterized by different statistical properties. According to the usual belief, all subclasses are still controlled by the same KPZ fixed point of renormalization group theory.

5.7. Height rescaling

In order to generalize the results (31) (44) (49) to other systems, we need to know how to rescale the height $h(x, t)$ and position x as functions of t . The procedure was established by Krug and coworkers [70, 71]. First of all, it is known that all statistical quantities in the KPZ scaling limit can be rescaled by using two parameters, A (as appeared in Eq. (8)) and λ . A can be estimated most straightforwardly from the height-difference correlation function

$$C_h(\ell, t) \equiv \langle [h(x + \ell, t) - h(x, t)]^2 \rangle \simeq A\ell, \quad (51)$$

which amounts to measuring the mean squared displacement of the Brownian stationary interfaces, Eq. (8). In general, for large t , the height profile becomes locally Brownian, so that Eq. (51) is valid up to the correlation length $\xi \sim t^{2/3}$. For the other parameter λ , if one has control over the global tilt of the interface²⁰ or knows the mean interface profile $\langle h(x, t) \rangle$, one can calculate the asymptotic growth speed $v_\infty(u) \equiv \lim_{t \rightarrow \infty} \langle \frac{\partial h}{\partial t} \rangle$ as a function of the tilt $u \equiv \lim_{t \rightarrow \infty} \langle \frac{\partial h}{\partial x} \rangle$ and use the following relation [70, 71]:

$$\lambda = \left. \frac{d^2 v_\infty(u)}{du^2} \right|_{u=0}. \quad (52)$$

In particular, if the interface grows isotropically in two-dimensional space at asymptotic speed v_∞ (as is the case in some experimental systems [29]), one simply has [19, 21]

$$\lambda = v_\infty. \quad (53)$$

As an alternative method, if one can control the system size L and measure the asymptotic growth speed $v_\infty(L)$ (in the direction normal to the interface) as a function of L , the following finite-size scaling can also be used [70, 71]:

$$v_\infty(L) - \lim_{L \rightarrow \infty} v_\infty(L) = -\frac{\lambda A}{2L}. \quad (54)$$

With the parameters A and λ , the evolution of the height $h(x, t)$ can be expressed as follows for large t :

$$h(x, t) \simeq v_\infty t + (\Gamma t)^{1/3} \chi(\zeta, t) \quad (55)$$

with

$$\Gamma \equiv \frac{1}{2} A^2 \lambda, \quad \zeta \equiv \frac{x}{\xi(t)} \equiv \frac{x}{2(\Gamma t)^{2/3}/A}. \quad (56)$$

The constant v_∞ can be determined directly from Eq. (55), by using²¹

$$\left\langle \frac{\partial h}{\partial t} \right\rangle \simeq v_\infty + (\text{const.}) \times t^{-2/3} \rightarrow v_\infty. \quad (57)$$

Then, Prähofer and Spohn [50] predicted that the statistical properties of the rescaled variable $\chi(\zeta, t)$ are universal within the KPZ class, despite the different distribution functions obtained for the different subclasses: in the limit $t \rightarrow$

²⁰ Numerically, one can use the shifted periodic boundary condition, $h(L, t) = h(0, t) + uL$.

²¹ One can plot $\langle \frac{\partial h}{\partial t} \rangle$ against $t^{-2/3}$, linearly extrapolate to $t \rightarrow \infty$, and read the y -intercept.

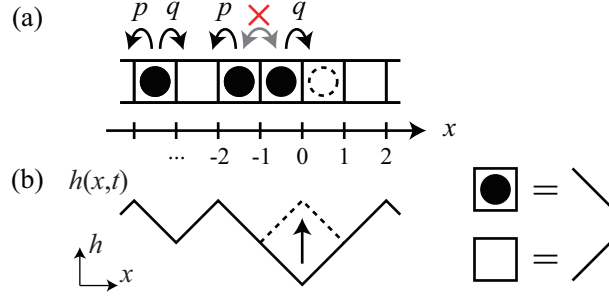


Figure 9: Definition of the 1D ASEP (a) and mapping to a surface growth problem (b).

$\infty, \chi(\zeta, t) \xrightarrow{d} \chi_0, \chi_1, \chi_2$ for the stationary, flat, and circular subclasses, respectively, where “ \xrightarrow{d} ” denotes convergence in the distribution.

To test this prediction, one can define the rescaled height

$$h_{\text{res}}(x, t) \equiv \frac{h(x, t) - v_{\infty}t}{(\Gamma t)^{1/3}} \simeq \chi(\zeta, t) \quad (58)$$

and measure its cumulants: the mean $\langle h_{\text{res}} \rangle$, the variance $\langle h_{\text{res}}^2 \rangle_c \equiv \langle \delta h_{\text{res}}^2 \rangle$ with $\delta h_{\text{res}} \equiv h_{\text{res}} - \langle h_{\text{res}} \rangle$, and the third- and fourth-order cumulants $\langle h_{\text{res}}^3 \rangle_c \equiv \langle \delta h_{\text{res}}^3 \rangle$ and $\langle h_{\text{res}}^4 \rangle_c \equiv \langle \delta h_{\text{res}}^4 \rangle - 3\langle \delta h_{\text{res}}^2 \rangle^2$, respectively. In practice, the mean $\langle h_{\text{res}} \rangle$ often includes a strong finite-time correction in the order of $\mathcal{O}(t^{-1/3})$ [21, 72, 73], which stems from the next leading order to Eq. (55), $\mathcal{O}(t^0)$. To reduce finite-time effect of $\langle h_{\text{res}} \rangle$, which is often problematic, one can also use [74]

$$\langle v_{\text{res}}(x, t) \rangle \equiv \frac{3t^{2/3}}{\Gamma^{1/3}} \left(\left\langle \frac{\partial h}{\partial t} \right\rangle - v_{\infty} \right) \simeq \langle \chi(\zeta, t) \rangle. \quad (59)$$

These rescaled cumulants can be directly compared with the known values of the cumulants [50] (Table 1 on p. 31) for the Baik-Rains (χ_0 , stationary), GOE Tracy-Widom (χ_1 , flat) and GUE Tracy-Widom distribution (χ_2 , circular)²².²³ Otherwise, amplitude ratios, such as skewness $\text{Sk}(h) \equiv \langle h^3 \rangle_c / \langle h^2 \rangle_c^{3/2} \simeq \text{Sk}(\chi)$ and kurtosis $\text{Ku}(h) \equiv \langle h^4 \rangle_c / \langle h^2 \rangle_c^2 \simeq \text{Ku}(\chi)$, are free from parameter estimation error. One may also try

$$\frac{9t^2 (\langle \frac{\partial h}{\partial t} \rangle - v_{\infty})^2}{\langle h^2 \rangle_c} = \frac{\langle v_{\text{res}} \rangle^2}{\langle h_{\text{res}}^2 \rangle_c} \simeq \frac{\langle \chi \rangle^2}{\langle \chi^2 \rangle_c}. \quad (60)$$

The advantage of this quantity is that only v_{∞} is needed, which may be estimated rather precisely by using Eq. (57).

6. Exact results on the 1D KPZ class 2: other important models and quantities

6.1. Asymmetric simple exclusion process

The asymmetric simple exclusion process (ASEP), one of the paradigmatic models in non-equilibrium statistical physics [75, 76], has also played a central role in the exact studies of the 1D KPZ class. The model is defined on a

²² Here are some pitfalls: (1) When comparing with the GOE Tracy-Widom distribution, be careful not to forget the factor $2^{-2/3}$ in Eq. (44). (2) To study the stationary subclass, one should use $h(x, t) - h(x, 0)$ instead of $h(x, t)$ (see footnote 17). (3) In this subsection we implicitly assume the translational symmetry in x . For the isotropically growing circular interfaces, one may use the local radius as the definition of the height and formally retrieve the translational symmetry (see Sec. 7).

²³ In practice, however, the precision of the parameter estimation by Eqs. (51)-(54) can be moderate, especially in experiments, due to finite-time effect and/or limited control over the experimental conditions (such as the tilt u and the system size L). In such a case, one may use one of the cumulants to determine the parameter Γ , by setting that cumulant in the rescaled unit to be one, or alternatively the known value of the expected distribution. The price to pay is, of course, one then abandons testing the theoretical prediction for that particular cumulant, but still the prediction can be tested with the other cumulants and other statistical quantities (such as correlation functions). It is not recommended to rescale the histogram in such a way that it has zero mean and unit variance, because it amounts to killing the two lowest-order cumulants; then the difference among χ_0, χ_1, χ_2 are often too small to detect from noisy data [29].

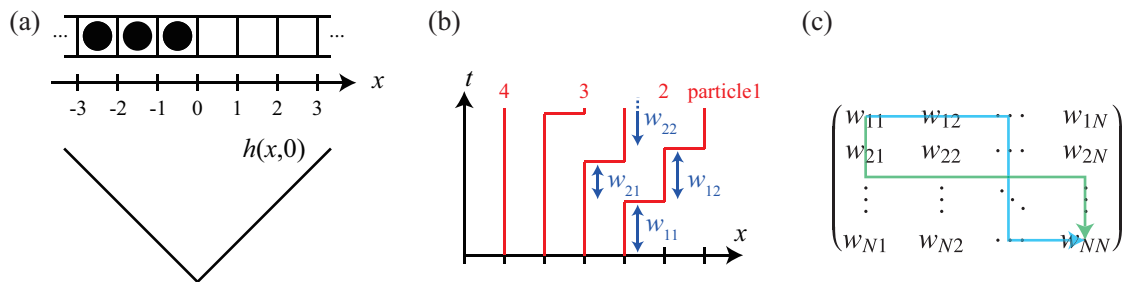


Figure 10: Outline of the TASEP problem solved by Johansson [49]. (a) Step initial condition and the corresponding initial interface profile. (b) Trajectories of particles and waiting times w_{ij} . (c) matrix of w_{ij} and last passage percolation.

lattice, here in 1D, with time $t \in \mathbb{R}$ and coordinate $x \in \mathbb{Z}$, which is assigned here to the midpoints of neighboring sites (Fig. 9(a)). Each site is either occupied by a particle or empty. Each particle can hop to a neighboring site stochastically and independently, on the right at rate q and on the left at rate p ($p < q$), unless the new site is already occupied by another particle. Since $q > p$, the particles flow on average to the right. The ASEP is therefore usually regarded as a model of stochastic particle transport. However, it can also be mapped to a model of interface growth, known by the name of single-step model in the literature, by replacing the occupied and empty sites with downward and upward slopes, respectively (Fig. 9(b)). Then a forward jump of a particle corresponds to local increase of the interface at that point (compare two sketches of Fig. 9). Therefore, the height increase, $h(x, t) - h(x, 0)$, is given by the total (net) number of particles that have passed the position x to the right. In other words, $h(x, t)$ is the integrated current, which tends to grow because of $q > p$. As expected from the evolution rule of the model, which consists of stochastic growth and local interactions (constraint that the interface slope is ± 1), ASEP is indeed in the KPZ class.

In fact, it is for the totally asymmetric version of ASEP (TASEP; $p = 0$) that the height distribution was first solved exactly, by Johansson in 2000 [49]. In the following we set $q = 1$ without loss of generality²⁴. We start from the step initial condition (Fig. 10(a)), where all sites with negative x are occupied and all sites with positive x are empty, and consider the number of particles that have passed $x = 0$ until time t , $N(t)$ ($= h(0, t)$). The quantity of interest is $\text{Prob}[N(t) \geq N]$. Then we notice that, in the case of TASEP, the proposition $N(t) \geq N$ is equivalent to the proposition $T_N \leq t$, where T_N is the time at which the N th particle from the front makes the N th hopping. This T_N can be written in terms of waiting times w_{ij} for the i th particle to make the j th hopping. If the waiting time w_{ij} is counted only while the i th particle is able to hop, i.e., while the next site is empty (see Fig. 10(b)), w_{ij} is simply an iid random number generated according to the exponential distribution, and T_N is given by²⁵

$$T_N = \max_{\pi \in \Pi} \sum_{(i,j) \in \pi} w_{ij}. \quad (61)$$

Here, Π is a set of paths in the matrix of w_{ij} that start from the top left corner w_{11} , run only rightward or downward, and reach the bottom right corner w_{NN} (Fig. 10(c)). Equation (61) is therefore a sort of optimization problem that maximizes the sum of w_{ij} along such a directed path, called the last passage percolation problem. We also notice that this is again a point-to-point problem of directed polymer (from the upper left to the lower right corner of the matrix w_{ij}) under random potential w_{ij} , akin to that considered for the circular PNG model (Fig. 5 and Eq. (29)).

Johansson [49] solved this problem using combinatorial techniques, namely the Young tableaux and the Robinson-Schensted-Knuth correspondence, and reached the following equation:

$$\text{Prob}[N(t) \geq N] = \text{Prob}[T_N \leq t] \propto \int_{[0,t]^N} \prod_{i=1}^N dx_i \prod_{i < j} (x_i - x_j)^2 \prod_i e^{-x_i}. \quad (62)$$

²⁴ Note that q is the rate and not the probability; with $q = 1$, each particle hops with probability dt (if it is allowed) during an infinitesimal time step dt .

²⁵ To understand Eq. (61), the reader is recommended to see Fig. 10(b) and confirm (diagrammatically) that $T_2 = \max\{w_{11} + w_{12} + w_{22}, w_{11} + w_{21} + w_{22}\}$.

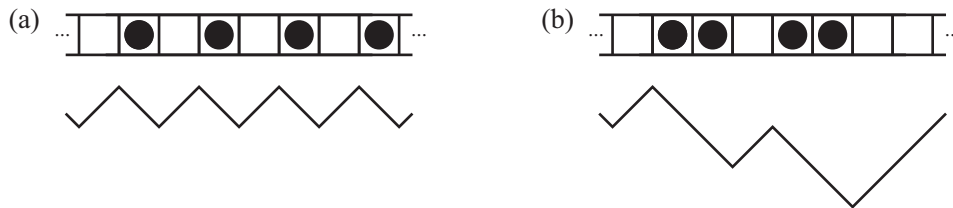


Figure 11: Representative initial conditions considered in ASEP, other than the step initial condition for the circular subclass, already shown in Fig. 10(a). (a) Alternating initial condition for the flat subclass. (b) Bernoulli initial condition for the stationary subclass. Here the particle configuration is generated randomly according to the Bernoulli measure; in other words, whether each site is occupied or empty is chosen randomly and independently with a fixed probability, $1/2$ in the case of the untilted stationary interface.

Remarkably, this equation is very similar to that of the largest eigenvalue of GUE random matrices, Eq. (38) with $\beta = 2$. Indeed, the slight difference between the two equations turned out to be irrelevant; $N(t)$, or the height $h(0, t)$, was shown to be²⁶

$$h(0, t) = N(t) \simeq \frac{t}{4} - 2^{-4/3} t^{1/3} \chi_2, \quad (63)$$

i.e., the height fluctuations show the GUE Tracy-Widom distribution. This is the characteristic distribution of the circular KPZ subclass. Why circular? One may guess that this is because of the global curvature of the interface, associated with the step initial condition (see Fig. 10(a)). But more appropriately, here the active region of the system, i.e., the region where particles exist and are not fully packed, expands in the course of time, just similarly to the nucleation region of the circular PNG problem (see Fig. 4(b)). Fluctuations then do not propagate along the h -axis, but rather in the radial direction (radial when properly rescaled). A related idea of direction of propagation was formulated mathematically, too, and called the characteristic line [77, 78].

With Johansson's result as the start, TASEP became one of the fundamental models to analyze rigorous properties of the 1D KPZ class. To study the flat subclass, one can use the alternating initial condition where empty and occupied sites are alternating (Fig. 11(a)), and the GOE Tracy-Widom distribution was indeed derived [79]. The stationary subclass can also be studied with the Bernoulli initial condition, where the occupation of each site is determined randomly and independently with a fixed probability ($1/2$ to generate an untilted stationary interface; Fig. 11(b)), and the Baik-Rains distribution was identified [80]. In contrast, solving the non-totally asymmetric case (i.e., $p \neq 0$) is much more difficult, because a property used in the mathematical results on TASEP, called free-fermionicity or complete determinantal structure, cannot be used. However, it was finally solved for the step initial condition (circular subclass) by Tracy and Widom [81] via a Bethe ansatz approach, and for the Bernoulli initial condition (stationary subclass) as well [82, 83] via relation to a variant of the six-vertex model.

From a different perspective, the type of optimization problems we considered in Eqs. (29) and (61) corresponds to the ground state of directed polymer, hence the zero-temperature problem. Its finite-temperature analogue, i.e.,

$$F = \frac{1}{\beta_T} \log Z, \quad Z = \sum_{\pi \in \Pi} \exp \left(-\beta_T \sum_{(i,j) \in \pi} E_{ij} \right) = \sum_{\pi \in \Pi} \prod_{(i,j) \in \pi} e^{-\beta_T E_{ij}} \quad (64)$$

has also been considered and for some models the Tracy-Widom distribution was indeed shown [84]. Moreover, in some quantum interference problems, a summation similar to Eq. (64) can arise over forward scattering paths in the Green function [85], but then $e^{-\beta_T E_{ij}}$ is replaced by a not necessarily positive factor. This arises for example in the context of conductance fluctuations of Anderson insulators, and interestingly the family of the Tracy-Widom distributions was still numerically observed [86, 87].

6.2. KPZ equation

The series of rigorous approaches to the PNG model, ASEP, and related models has finally led to exact solutions to the 1D KPZ equation (as defined in Eq. (27) with the 1D stochastic heat equation (26)), first in the year 2010. An

²⁶ Johansson [49] obtained a formula for general x , but for the sake of simplicity only the result for $x = 0$ is shown here.

important background was Tracy and Widom's solution of the (non-totally) ASEP [81], because the KPZ equation is actually known to be linked to certain weak asymmetric limit of ASEP [43–46]. More specifically, set the hopping rates of ASEP to satisfy $q - p = a\sqrt{\varepsilon}$ with asymmetry parameter $\varepsilon \ll 1, a > 0$, and $p + q = 1$, and denote the height profile of ASEP by $h_{\text{ASEP}}^\varepsilon(x, t)$ (as illustrated in Fig. 9). Then, it was shown that $\sqrt{\varepsilon}h_{\text{ASEP}}^\varepsilon(\lfloor \varepsilon^{-1}x \rfloor, \varepsilon^{-2}t)$ in the limit $\varepsilon \rightarrow 0$ corresponds to the height of the KPZ equation with $\nu = 1/2, \lambda = D = 1$, $h_{\text{KPZ}}(x, t)$, up to some shifts. The combination of this correspondence and the developments by Tracy and Widom on ASEP with the step initial condition, with other mathematical elaborations, led Sasamoto and Spohn [44, 45] and independently Amir *et al.* [46] to establish the exact solution of the 1D KPZ equation for the narrow-wedge initial condition:

$$h(x, 0) = -\lim_{\delta \rightarrow 0^+} \frac{|x|}{\delta} = \begin{cases} 0 & (x = 0), \\ -\infty & (x \neq 0), \end{cases} \quad Z(x, 0) \propto \delta(x). \quad (65)$$

The exact solution consists of an analytic expression for the one-point distribution of $h(x, t)$, which indeed converges to the GUE Tracy-Widom distribution of the circular KPZ subclass (in the rescaled unit).

Almost simultaneously, another approach based on the correspondence to the directed polymer problem and the use of the Bethe ansatz [88] was established by Calabrese *et al.* [51] and by Dotsenko [52]. To see this connection, let us first simplify the notation of the KPZ equation (10) by the following transformation

$$x \mapsto \frac{(2\nu)^3}{D\lambda^2}x, \quad t \mapsto \frac{(2\nu)^5}{D^2\lambda^4}t, \quad h \mapsto \frac{2\nu}{\lambda}h. \quad (66)$$

This amounts to setting $\nu = 1/2, \lambda = D = 1$ in the KPZ equation, without loss of generality, and the newly defined x, t, h are dimensionless quantities. Then we start from the stochastic heat equation (26) with smoothed noise $\eta_\kappa(x, t)$ defined in Eqs.(22) and (23) (with $D = 1$). When converted to the Stratonovich form through Eqs. (24) and (25), it reads:

$$\frac{\partial}{\partial t}Z(x, t) = \frac{1}{2}\nabla^2Z(x, t) + \eta_\kappa(x, t) \circ Z(x, t) - \frac{1}{2}\Delta_\kappa(0)Z(x, t). \quad (67)$$

This has a form similar to the Schrödinger equation; then the solution $Z(x, t)$ of such an equation can be described by a path integral à la Feynman. Indeed, according to the Feynman-Kac formula²⁷ [89], the path integral expression of $Z(x, t)$ is given by

$$\begin{aligned} Z(x, t) &= \int dx_0 Z(x_0, 0) \int_{B(0)=x_0}^{B(t)=x} \mathcal{D}B(\tau) \exp \left\{ - \int_0^t d\tau \left[\frac{1}{2} \left(\frac{dB}{d\tau} \right)^2 - \eta(B(\tau), \tau) + \frac{1}{2} \Delta_\kappa(0) \right] \right\} \\ &= \int dx_0 Z(x_0, 0) \int_{B(0)=x_0}^{B(t)=x} \mathcal{D}B(\tau) e^{-E_{\text{DP}}[B(\tau)]} \end{aligned} \quad (70)$$

with

$$E_{\text{DP}}[B(\tau)] = \int_0^t d\tau \left[\frac{1}{2} \left(\frac{dB}{d\tau} \right)^2 - \eta(B(\tau), \tau) + \frac{1}{2} \Delta_\kappa(0) \right]. \quad (71)$$

Here, the endpoints of the path $B(\tau)$ are fixed at $B(0) = x_0$ and $B(t) = x$ in the path integral, but the first endpoint

²⁷ The Feynman-Kac formula tells us that the solution of

$$\frac{\partial Z}{\partial t} = \nu \frac{\partial^2 Z}{\partial x^2} + U(x, t)Z(x, t) \quad (68)$$

with initial condition $Z(x, 0) = \delta(x - x_0)$ is given by path integral

$$Z(x, t) = \int_{B(0)=x_0}^{B(t)=x} \mathcal{D}B(\tau) \exp \left\{ - \int_0^t d\tau \left[\frac{1}{4\nu} \left(\frac{dB}{d\tau} \right)^2 - U(B(\tau), \tau) \right] \right\}, \quad (69)$$

where the two endpoints of the path $B(\tau)$ are fixed at $B(0) = x_0$ and $B(t) = x$. If $U(x, t) = 0$, Eq. (68) is the diffusion equation, and the resulting path integral (69) is simply the probability measure of Brownian motion; in other words, $B(\tau)$ can be regarded as Brownian motion, as naturally expected. Now, with $U(x, t)$, the second term of Eq. (68) introduces exponential variation of the statistical weight $Z(x, t)$, which indeed appears in the action of Eq. (69). Of course, this is merely an interpretation; one should check the derivation of the formula to be convinced [89].

x_0 is distributed according to the probability density $\propto Z(x, 0) = e^{h(x, 0)}$. Importantly, Eq. (70) can be interpreted as the partition function of a directed polymer $B(\tau)$ – directed since time only increases –, with energy $E_{\text{DP}}[B(\tau)]$ and temperature $k_B T = 1$. According to Eq. (71), its energy per unit length along the τ -axis consists of elastic energy $\frac{1}{2} \left(\frac{dB}{d\tau} \right)^2$ and random potential $-\eta(x, t)$ (plus $\frac{1}{2} \Delta_\kappa(0)$). The height $h(x, t) = \log Z(x, t)$ is then the (minus) free energy of the directed polymer. Further, for the narrow-wedge initial condition (65) (i.e., the circular subclass), the initial endpoint of the polymer is fixed at $(x, t) = (0, 0)$; therefore, it is again the point-to-point problem. For the flat case, the initial condition $Z(x, 0) = e^{h(x, 0)}$ is constant, so that the initial endpoint of the polymer is uniformly distributed along the line $t = 0$. This is the point-to-line problem, analogous to the flat case of the PNG model [Sec. 5.4 and Fig. 7(a)].

To investigate the fluctuations of $h(x, t)$, or equivalently $Z(x, t)$, one may examine the moments $\langle Z(x_1, t) Z(x_2, t) \cdots Z(x_N, t) \rangle$, which amounts to considering replicas of $Z(x, t)$. Here the ensemble average is taken over noise realizations $\eta_\kappa(x, t)$. Therefore, with $x_n(\tau)$ being the trajectory $B(\tau)$ of the n th replica and $\eta_n \equiv \eta_\kappa(x_n(\tau), \tau)$, the random potential contribution in Eq. (70) during the time interval $[\tau, \tau + d\tau)$ can be evaluated as follows:

$$\langle e^{\sum_n \eta_n d\tau} \rangle = \int \left(\prod_n d\eta_n \right) e^{\sum_n \eta_n d\tau} \exp \left(\sum_{n,m} \frac{\eta_n \eta_m}{2 \Delta_\kappa(x_n - x_m) / d\tau} \right) \propto \exp \left(\frac{1}{2} \sum_{n,m} \Delta_\kappa(x_n - x_m) d\tau \right), \quad (72)$$

where the right hand side is obtained by the Gauss integral over η_n . Then we have

$$\langle Z(x_1, t) Z(x_2, t) \cdots Z(x_N, t) \rangle \propto \int \left(\prod_n dx_{n0} Z(x_{n0}, 0) \right) \int_{x_n(0)=x_{n0}}^{x_n(t)=x_n} \left(\prod_n \mathcal{D}x_n(\tau) \right) \exp \left\{ - \int_0^t d\tau \left[\frac{1}{2} \sum_n \left(\frac{dx_n}{d\tau} \right)^2 - \frac{1}{2} \sum_{n \neq m} \Delta_\kappa(x_n - x_m) \right] \right\}, \quad (73)$$

where trajectories $x_n(\tau)$ are initially distributed according to $Z(x, 0)$ (expressed by the first integral) and arrive at $x_n(t) = x_n$. Now we switch to the quantum mechanics representation. By applying the Feynman-Kac formula to this many-body problem, now from the path-integral representation (73) back to the partial differential equation, we obtain the following Schrödinger-like equation

$$\frac{\partial}{\partial t} \Psi(\mathbf{x}, t) = \left[\frac{1}{2} \sum_n \frac{\partial^2}{\partial x_n^2} + \frac{1}{2} \sum_{n,m} \Delta_\kappa(x_n - x_m) \right] \Psi(\mathbf{x}, t) \equiv -\hat{H}_\kappa \Psi(\mathbf{x}, t) \quad (74)$$

with $\mathbf{x} \equiv (x_1, \dots, x_N)$ and Hamiltonian

$$\hat{H}_\kappa \equiv -\frac{1}{2} \sum_n \frac{\partial^2}{\partial x_n^2} - \frac{1}{2} \sum_{n \neq m} \Delta_\kappa(x_n - x_m). \quad (75)$$

The KPZ equation is retrieved by $\kappa \rightarrow 0$. Therefore, the corresponding Hamiltonian is

$$\hat{H}_{\text{LL}} = -\frac{1}{2} \sum_n \frac{\partial^2}{\partial x_n^2} - \frac{1}{2} \sum_{n \neq m} \delta(x_n - x_m) \quad (76)$$

and the cumulants can be expressed as follows by using the quantum mechanics representation:

$$\langle Z(x_1, t) Z(x_2, t) \cdots Z(x_N, t) \rangle = \langle \mathbf{x} | e^{-\hat{H}_{\text{LL}} t} | \mathbf{x}_0 \rangle, \quad (77)$$

where $|\mathbf{x}_0\rangle$ represents the initial condition ($|\mathbf{0}\rangle$ for the narrow-wedge case). The Hamiltonian (76) describes bosons with contact interactions, known as (the attractive version of) the Lieb-Liniger model [90]. It is a well-known integrable system [88], which has also an experimental relevance as recently demonstrated by experiments on the Bose-Einstein condensation of cold atom gas for the repulsive case [91, 92]. It is interesting that the KPZ problem is linked to such an apparently distinct problem.

From the theoretical viewpoint, this connection to the Lieb-Liniger model is important, because one can employ the Bethe ansatz [88] to carry out the computation of the cumulants $\langle Z(0, t)^n \rangle_c$ from Eq. (77) [51–54]. Although in

general the conversion from cumulants to distribution is not unique, and even worse in the present problem a rapidly diverging term appears, which cannot be treated with mathematical rigor, this approach successfully gave the GUE Tracy-Widom distribution for the narrow-wedge initial condition [51, 52]. This method also seems to be versatile; it was adapted to other initial conditions as well, and indeed, the GOE Tracy-Widom distribution was found for the flat case $h(x, 0) = 0$ [53] and the Baik-Rains distribution for the stationary initial condition $h(x, 0) = \sqrt{AB(x)}$ (Eq. (8)) with $h(0, 0) = 0$ [54]. The stationary result was also proved mathematically later [55]. Now, there are a number of mathematical approaches to study the KPZ equation (a nice summary can be found in introduction of [55]), which have deepened the mathematical understanding of this equation even more. In the meantime, the replica Bethe ansatz approach continues being a powerful method of theoretical physics, which allows us to compute a variety of statistical quantities.

6.3. Spatial correlation

So far we have focused on the one-point distribution of $h(x, t)$, but it is by no means the only quantity studied in recent developments on exact solutions. Among others, one of the most important statistical properties that have been deeply understood is the spatial correlation, e.g., joint distribution of $h(x, t)$ at multiple points x_1, x_2, \dots at a single time t . It is usually described by the rescaled coordinates, in other words, in terms of the rescaled height profile $\chi(\zeta, t)$ defined by Eq. (55). In the limit $t \rightarrow \infty$, the joint distribution of $\chi(\zeta, t)$ becomes independent of t . Consequently, $\chi(\zeta, \infty)$ can be regarded as a “stochastic process”, with ζ playing the role of time for this process. It is analogous to the way the stationary interface profile of the 1D KPZ equation was described by a Brownian motion in Eq. (8). Then the spatial correlation properties of KPZ-class interfaces can be expressed as the time correlation properties of such stochastic processes.

Analytic expressions for such limiting processes have been obtained for the the circular and flat subclasses [93], and named the Airy₂ process $\mathcal{A}_2(\zeta)$ for the circular case [66, 94] and the Airy₁ process $\mathcal{A}_1(\zeta)$ for the flat case [79, 95]. More specifically, $\chi(\zeta, t)$ is predicted to converge as follows:

$$\chi(\zeta, t) \xrightarrow{d} \begin{cases} \mathcal{A}_2(\zeta) - \zeta^2 & (\text{circular subclass}) \\ \mathcal{A}_1(\zeta) & (\text{flat subclass}) \end{cases} \quad (t \rightarrow \infty) \quad (78)$$

where “ \xrightarrow{d} ” now denotes convergence of multi-point distributions and the term $-\zeta^2$ in the circular case comes from the curvature of the circular interfaces²⁸. As such, the one-point distribution of $\mathcal{A}_i(\zeta)$ is simply the distribution of χ_i , namely the GUE and GOE Tracy-Widom distributions ($i = 2$ and 1 , respectively). For the stationary subclass, a similarly defined limiting process would be just the Brownian motion (Eq. (8)); therefore, one can consider instead [96]

$$\chi_{\text{stat}}(\zeta, t) \equiv (\Gamma t)^{-2/3} \langle (h(x, t) - h(0, 0) - v_\infty t)^2 \rangle. \quad (79)$$

For this object, the limiting process $\mathcal{A}_{\text{stat}}(\zeta)$, named the Airy_{stat} process, was indeed formulated [97].

Interestingly, a direct connection between the Airy₂ process and GUE random matrices is also known: the former is actually equivalent to a time-dependent process of a GUE random matrix [66, 93], called Dyson’s Brownian motion. In this model, each element of an $N \times N$ GUE matrix $M(t)$ (Eq. (32)) is assumed to perform an independent Ornstein-Uhlenbeck process [57, 58], that is,

$$\frac{dM(t)}{dt} = -M(t) + \Xi(t), \quad (80)$$

where $\Xi(t)$ is a Hermitian matrix with white Gaussian noise elements $\Xi_{ij}(t)$, whose mean is $\langle \Xi_{ij}(t) \rangle = 0$ and covariance is $\langle \Xi_{ii}(t) \Xi_{i'i'}(t) \rangle = \delta_{ii'} \delta(t - t')$ for the diagonal elements and $\langle [\text{Re } \Xi_{ij}(t)] [\text{Re } \Xi_{i'j'}(t)] \rangle = \langle [\text{Im } \Xi_{ij}(t)] [\text{Im } \Xi_{i'j'}(t)] \rangle = (1/2) \delta_{ii'} \delta_{jj'} \delta(t - t')$ for the non-diagonal elements ($i < j, i' < j'$). Then we focus on its largest eigenvalue $\lambda_{\text{max}}(t)$ and, analogously to the one-point rescaling given in Eq. (39), it was shown to converge to the Airy₂ process [66, 93] as

$$2^{1/2} N^{1/6} \left[\lambda_{\text{max}}(\zeta/N^{1/3}) - \sqrt{2N} \right] \xrightarrow{d} \mathcal{A}_2(\zeta). \quad (81)$$

²⁸ In relation to the factor $2^{-2/3}$ between χ_1 and $\chi_{\text{TW},1}$ in Eq. (44), the Airy₁ process $\mathcal{A}_1(\zeta)$ can be normalized differently, in such a way that $\chi(\zeta, t)$ converges to $2^{1/3} \mathcal{A}_1(2^{-2/3} \zeta)$ [68, 93]. In these lecture notes, however, we adopt the normalization that satisfies Eq. (78), which is simpler in the KPZ context.

One might also expect a similar relationship between the Airy_1 process and Dyson's Brownian motion for GOE random matrices, but curiously the two processes are not the same [98]. In other words, the mathematical structure behind the 1D KPZ class does *not* overlap entirely with random matrix theory.

From a practical viewpoint, a useful quantity to characterize the spatial correlation is the two-point correlation function, defined by

$$C_s(\ell, t) \equiv \langle h(x + \ell, t)h(x, t) \rangle_c \equiv \langle \delta h(x + \ell, t)\delta h(x, t) \rangle \quad (82)$$

with $\delta h(x, t) \equiv h(x, t) - \langle h(x, t) \rangle$. According to Eqs. (55) and (56), the correlation function may be rescaled as follows and is expected to converge to the two-point correlation of the corresponding Airy process²⁹:

$$C_{s,\text{res}}(\zeta, t) \equiv (\Gamma t)^{-2/3} C_s(\zeta \cdot \xi(t), t) \xrightarrow{d} g_i(\zeta) \equiv \langle A_i(\zeta)A_i(0) \rangle_c. \quad (83)$$

Strikingly, the Airy correlation functions $g_i(\zeta)$ are known to decay in *qualitatively* different manners: while the spatial correlation of the circular subclass decays by a power law, $g_2(\zeta) \sim \zeta^{-2}$ [98, 99], that of the flat subclass decays superexponentially, specifically, $g_1(\zeta) \sim e^{-c_1|\zeta|^3}$ with constant c_1 [98, 100]. This is in contrast to the fact that the GUE and GOE Tracy-Widom distributions are only quantitatively different (see Fig. 6). For the stationary subclass, too, the two-point function defined analogously [96] decays superexponentially, $g_0(\zeta) \sim e^{-c_0|\zeta|^3}$ with a coefficient c_0 different from c_1 .

In contrast to spatial correlations, correlation properties in time have remained an analytically challenging problem, but a few results started to emerge very recently [101–105]. We shall come back to this point in Sec. 7.4.

7. Liquid crystal experiment

While the recent developments on the 1D KPZ problem have been mostly driven by mathematical approaches, the obtained results have striking physical implications and the quantities of interest are, at least in principle, observable in experiments and simulations. Testing universality of the wealth of mathematical results is crucial, because essentially all those developments rely on the integrability of the studied models, which constitute only a special group of systems in the large KPZ universality class. Experimentally, as already noted in footnote 4, even the scaling exponents of the KPZ class have been rarely found [29], the first examples being growing interfaces of mutant bacteria colony [106] and slow combustion of paper [107, 108]. Recently, however, a growing number of experiments have been reported, in which the two independent exponents of the 1D KPZ class were clearly observed [29]. Here we focus on one such experiment, namely that on growing interfaces in liquid crystal turbulence conducted by Takeuchi and Sano [19–21]. This experiment was able to provide sufficient accuracy to study fine statistical quantities, such as the distribution and correlation functions. For the description of other experimental systems, the readers are kindly referred to the author's recent review [29] and references therein.

7.1. Experimental system

The system to study is electroconvection of nematic liquid crystal [109], i.e., convection driven by an electric field applied between two parallel glass plates (Fig. 12(a)). In the standard setup, the surface alignment of liquid crystal is set to be parallel to the glass plates (planar alignment). Electroconvection is observed if the liquid crystal has the following type of anisotropy in material properties: $\varepsilon_{\parallel} < \varepsilon_{\perp}$ in the dielectric constants and $\sigma_{\parallel} > \sigma_{\perp}$ in the conductivity, where \parallel and \perp indicate the directions with respect to the alignment of liquid crystal, or the director field. The mechanism is described by the Carr-Helfrich theory [109] in the case of the weak ac field at relatively low frequencies, as illustrated in Fig. 12(b) with explanations in its caption. Increasing the applied voltage V , one can observe a series of different patterns and finally reaches a regime of spatiotemporal chaos, or turbulence, called the dynamic scattering mode (DSM) [109]. There are two turbulent regimes here, called DSM1 and DSM2. DSM2 is observed under higher voltages and composed of topological defect lines as sketched in Fig. 13(a). More precisely, on applying a sufficiently high electric field, one first observes the DSM1 state, but it is only metastable and eventually

²⁹ According to [98], a numerical table of $g_1(\zeta)$ and $g_2(\zeta)$ can be obtained from Bornemann by his courtesy. Be aware of the different definition of $\mathcal{A}_1(\zeta)$ as stated in footnote 28.

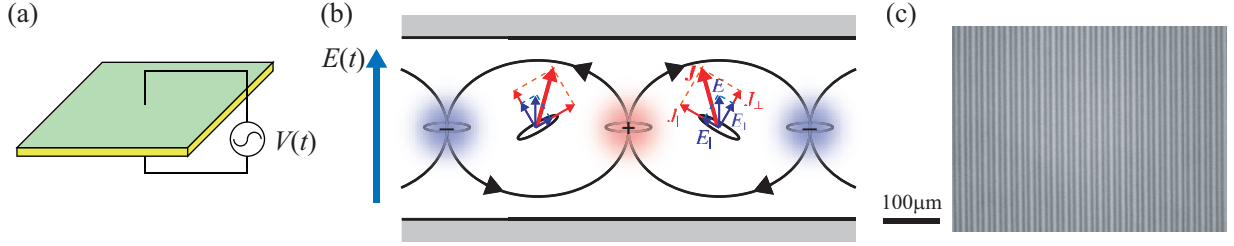


Figure 12: Sketch of the experimental system of liquid crystal electroconvection (a) and the Carr-Helfrich mechanism for roll convection (b), which looks as in (c). (a) The system consists of nematic liquid crystal between two parallel glass plates, coated with transparent electrodes. The gap is typically 10 to 50 μm and the span-wise size is about 1 cm. For the experiment described in this note [20, 21], it is 12 μm and 16 mm, respectively. (b) This panel shows a side view of the system. In the planar alignment condition and in the absence of field, liquid crystal molecules in bulk are also aligned in a direction parallel to the surfaces. Now, under a weak ac field $E(t)$, we consider a small perturbation of the director field as sketched (by the tilted ellipsoids), which is taken to be a single Fourier component. Since the director field is now not perpendicular to the electric field, to use Ohm's law, we need to decompose the electric field into the components parallel and normal to the director field, E_{\parallel} and E_{\perp} , respectively, and apply Ohm's law to each component. Because of $\sigma_{\parallel} > \sigma_{\perp}$, the induced current \mathbf{J} has a lateral component, which leads to spatially periodic concentration of positive and negative charges. Those charges are also subjected to the field, positive charges forced upward and negative ones downward, hence generating circular flow as shown in the panel. This flow exerts a torque to the molecules, in the direction that amplifies the considered perturbation. There is also an effect from the anisotropic dielectric constants $\epsilon_{\parallel} < \epsilon_{\perp}$, which also favors the deformed director field. The amplitude of the deformation is determined by the balance of those effects and the nematic elasticity. Since the electric field is ac, its direction oscillates periodically. At low frequencies considered here, the currents and charges are oscillating with the external field, while the flow and the director field remain static. See [109] for more detailed descriptions of the mechanism described here. (c) A microscope image of the roll convection. The anisotropic refractive index of liquid crystal allows us to observe the convection pattern by the simple bright-field microscopy (i.e., by the transmitted light) [109], without the need for tracer particles.

replaced by the stable DSM2 state. Here, DSM2 nucleates randomly and takes over the metastable DSM1 state through a random growth process, as shown in Fig. 13(b,c). It is this process that we focus on here, in the context of kinetic roughening of interfaces. Observations suggest that topological defects are stretched, multiplied (through broken alignment anchoring at the glass surfaces), and randomly transported by local turbulent flow, which result in random growth of DSM2 in macroscopic scales. The interactions are expected to be short-ranged, because DSM2 is a regime of spatiotemporal chaos³⁰, where correlation of flow fluctuations decays exponentially in space and time.

To work with the simplest situation of isotropic growth, Takeuchi and Sano [19–21] chose to use the so-called homeotropic alignment, where surface alignment of liquid crystal is perpendicular to the glass surfaces. They also decided not to rely on spontaneous DSM2 nucleation, but rather to trigger it, by shooting ultraviolet laser pulses. Figure 13(b) shows a DSM2 interface, generated by pulses shot to a central point of the system, hence the interface is circular. Moreover, by expanding the laser beam in one direction, they also shot pulses along a line, which then generates a flat interface (Fig. 13(c)). This ability to change the interface geometry is important to test the theoretical hypothesis on the existence of different universality subclasses. With the help of accurate temperature control, the authors were able to obtain 955 circular and 1128 flat interfaces under practically the same experimental conditions [21]. Then they defined the height $h(x, t)$ as illustrated in Fig. 13(b,c). For the circular case, $h(x, t)$ was chosen to be the local radius of the interface. In this way, one can use data at all angular positions to evaluate statistical quantities, whereas the actual spatial coordinate is the azimuth θ (Fig. 13(b)). In the following, however, x is still used as the coordinate, which is formally converted by $x = \langle h \rangle \theta$. Then it turned out that the Family-Vicsek scaling (1) was accurately confirmed for both circular and flat interfaces, with the exponents α, β, z in agreement with the 1D KPZ class [19–21].

7.2. Distribution

With the data obtained thereby, the authors first measured the skewness $\text{Sk}(h) = \langle h^3 \rangle_c / \langle h^2 \rangle_c^{3/2}$ and kurtosis $\text{Ku}(h) = \langle h^4 \rangle_c / \langle h^2 \rangle_c^2$, which do not require estimation of the scaling coefficients. Then significant differences were found

³⁰ One can roughly estimate the Reynolds number for the DSM turbulence at $\text{Re} \approx 10^{-6} \ll 1$, using tens of micrometers as typical length scale, tens of micrometers per second as velocity scale, and known values of viscosities of nematic liquid crystal used here, namely MBBA [109]. Therefore, DSM2 is by no means a fully developed turbulence which would have long-ranged correlation.

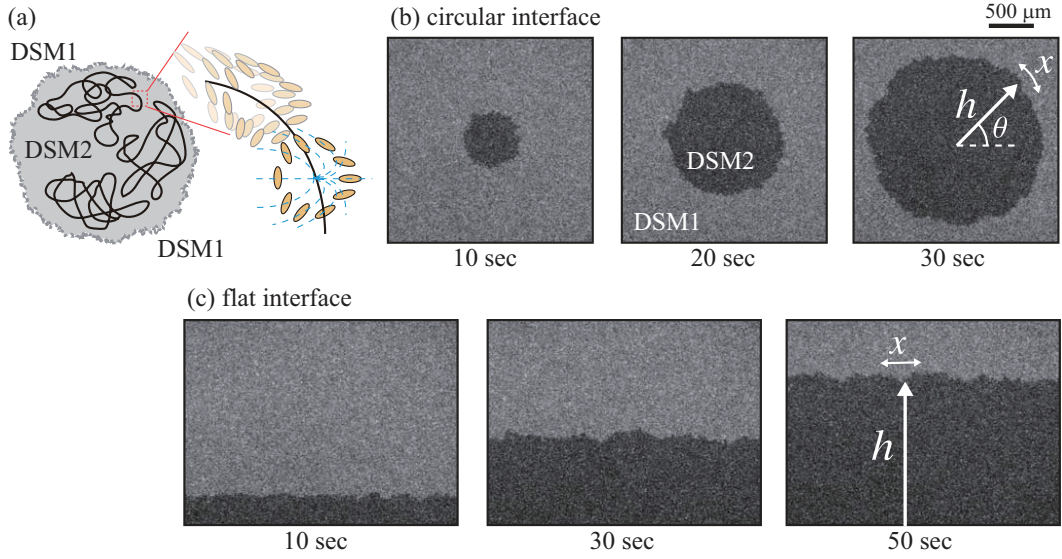


Figure 13: (a) Sketch of the DSM2 state which consists of topological defects, specifically disclination lines, in the nematic director field. Such defects are absent in the DSM1 state. (b,c) Snapshots of growing DSM2 clusters under homeotropic alignment. The growth was triggered by shooting laser pulses, either to a point or to a line, hence generating circular (b) and flat (c) interfaces, respectively [21]. Time is measured from the emission of laser pulses. Reprints with permission from [21] with some adaptations.

between the circular and flat interfaces, which were moreover in agreement with the values of the GUE and GOE Tracy-Widom distributions, respectively (Fig. 14(a)). The circular and flat interfaces indeed show different fluctuation properties.

To make a more direct comparison with the Tracy-Widom distributions, the authors evaluated scaling coefficients by the method described in Sec. 5.7. By Eq. (57), the parameter ν_∞ was precisely estimated with four significant digits (Fig. 14(b) inset for the circular case). Thanks to the rotational symmetry of the system, $\lambda = \nu_\infty$ (Eq. (53)). In contrast, the parameter A could be determined from the height-difference correlation function $C_h(\ell, t) \simeq A\ell$ (Eq. (51)) only with two significant digits (Fig. 14(b) main panel), because of the rather narrow region in which the scaling (51) appears, as well as finite-time effect. This restricted the precision of $\Gamma = A^2\lambda/2$ as well. However, because it was already good enough to distinguish the GUE and GOE Tracy-Widom distributions, the authors took the variance $\langle h^2 \rangle_c \simeq (\Gamma t)^{2/3} \langle \chi_i^2 \rangle_c$ and used the variance of χ_2 and χ_1 to improve the precision of Γ [21] (see also footnote 23). The parameter A was obtained in turn by $A = \sqrt{2\Gamma/\lambda}$.

With these scaling coefficients, the authors obtained the rescaled height h_{res} by Eq. (58) and constructed the histogram (Fig. 14(c)). The results clearly confirmed the GUE and GOE Tracy-Widom distributions, apart from a small horizontal shift due to finite-time corrections. Indeed, by plotting $\langle h_{\text{res}}^n \rangle_c - \langle \chi_i^n \rangle_c$ with $i = 2$ (circular) and $i = 1$ (flat), the authors found that the mean ($n = 1$) has a pronounced finite-time correction³¹ that decays as $t^{-1/3}$, while the corrections in the other cumulants became small enough during the observation time. In summary, the emergence of the Tracy-Widom distributions, as well as the split into the circular and flat subclasses, were clearly found in this experiment. Those results turned out not to be special properties of integrable systems, but universal features of the KPZ class!

7.3. Spatial correlation

The scaling coefficients Γ and λ are also sufficient to test the predictions on the spatial correlation (Sec. 6.3). The authors measured the two-point spatial correlation function $C_s(\ell, t)$ (Eq. (82)) and rescaled it according to Eq. (83). The rescaled function $C_{s,\text{res}}(\zeta, t)$ was then plotted against rescaled length ζ (Fig. 15) and excellent agreement was

³¹ The presence of the correction $\sim t^{-1/3}$ in the mean $\langle h_{\text{res}} \rangle$ can be easily understood as a contribution from the next leading term in Eq. (55), which is $O(t^0)$.

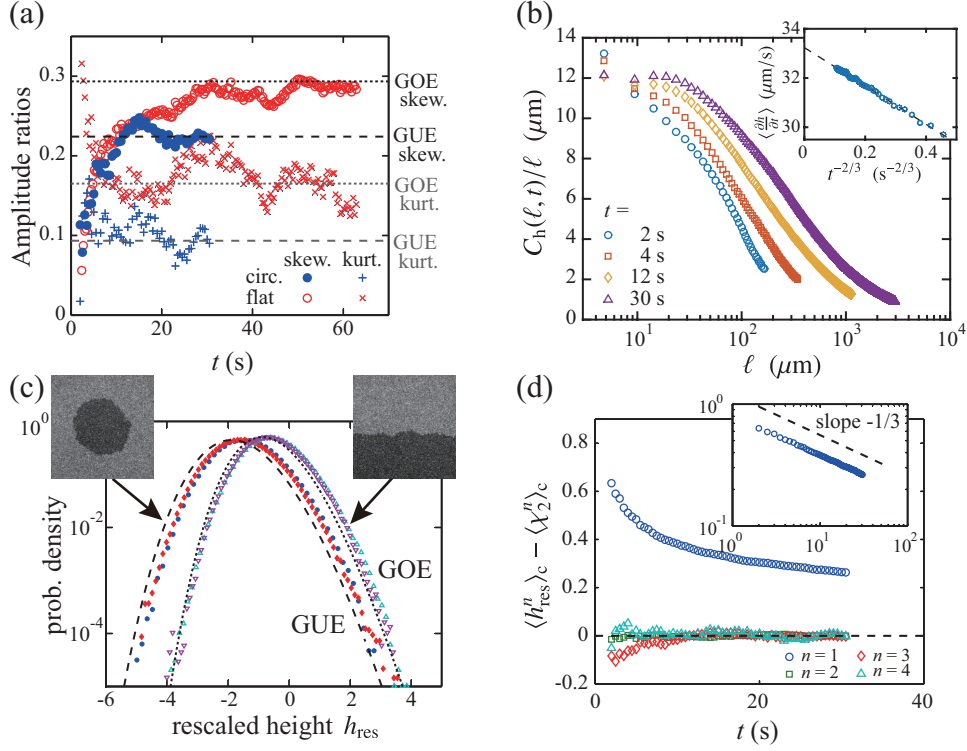


Figure 14: Experimental results of the one-point distribution [20, 21]. (a) Skewness $Sk(h)$ and kurtosis $Ku(h)$ as functions of time. (b) The height-difference correlation function $C_h(\ell, t)$ divided by ℓ (main panel) and the mean growth speed $\langle \frac{\partial h}{\partial t} \rangle$ (inset) in the circular case. (c) Histograms of rescaled height h_{res} for the circular case (solid symbols; $t = 10$ s (blue \bullet) and $t = 30$ s (red \blacklozenge)) and for the flat case (open symbols; $t = 20$ s (turquoise \triangle) and $t = 60$ s (purple ∇)). Those are compared with the GUE and GOE Tracy-Widom distributions (dashed and dotted lines, respectively). (d) Finite-time corrections in the n th-order cumulant h_{res} for the circular case. The inset shows the correction for the mean in the log-log scales. Reprints with permission from [21] (a,c) and from [20] (d) with some adaptations.

found with the Airy_2 correlation $g_2(\zeta)$ for the circular case³², and with the Airy_1 correlation $g_1(\zeta)$ for the flat case. This implies that the interface profiles we can observe by microscope, i.e., Fig. 13(b,c), are nothing but realizations of the Airy_2 and Airy_1 processes (circular and flat interfaces, respectively) at large t . More importantly, the agreement with them also implies that the qualitatively different decay of the spatial correlation function is also present in this experimental system (see discussions below Eq. (83)).

7.4. Temporal correlation

In contrast to the theoretically well-understood spatial correlation, temporal correlation has remained a very difficult property to study analytically. However, experimentally, it is one of the natural and straightforward quantities to measure. It is quantified here by the two-time correlation function³³

$$C_t(t_1, t_2) \equiv \langle h(x, t_1)h(x, t_2) \rangle_c. \quad (84)$$

According to the usual scaling ansatz, it is expected to scale as $C_t(t_1, t_2) \simeq (\Gamma^2 t_1 t_2)^{1/3} F_t(t_2/t_1)$ with a scaling function $F_t(\cdot)$. Therefore, one can define the rescaled two-time function by

$$C_{t,res}(t_1, t_2) \equiv (\Gamma^2 t_1 t_2)^{-1/3} C_t(t_1, t_2) \simeq F_t(t_2/t_1). \quad (85)$$

³² Note that, thanks to the use of the rescaled radius for the circular case, one does not need to take into account the influence of the global curvature, so that the term $-\zeta^2$ in Eq. (78) is omitted and one can directly compare with the function $g_2(\zeta)$.

³³ Note that for the circular case the azimuth θ was actually fixed in Eq. (84).

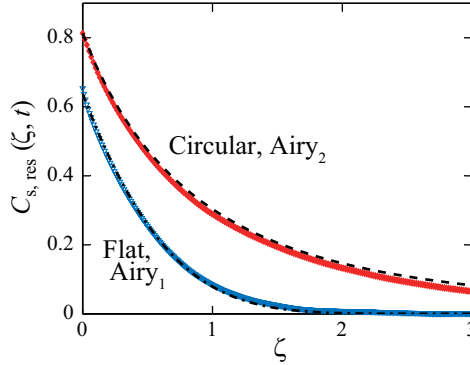


Figure 15: Experimental results for the spatial correlation function [21]. The rescaled correlation function $C_{s, \text{res}}(\zeta, t)$ as defined in Eq. (83) is shown against rescaled length $\zeta = (A\ell/2)(\Gamma t)^{-2/3}$, for the circular case (red solid symbols; $t = 30$ s) and for the flat case (blue open symbols; $t = 60$ s). The data are compared with the two-point function of the Airy_2 correlation $g_2(\zeta)$ (dashed line) and the Airy_1 correlation $g_1(\zeta)$ (dashed-dotted line). Reprints with permission from [21] with some adaptations.

Figures 16(a,b) show the experimental results for the flat (a) and circular (b) interfaces. The scaling (85) is confirmed in the insets, despite somewhat larger finite-time correction for the circular case. Here we notice an important difference between the two cases: when t_2 is increased with fixed t_1 , the correlation $C_t(t_1, t_2)$ decays as usually expected in the flat case (Fig. 16(a)), but in the circular case it decays very slowly and remains large during the observation time (Fig. 16(b)). Indeed, while the rescaled function decays as $F_t(\tau) \sim \tau^{-\bar{\lambda}}$ with $\bar{\lambda} = 1$ for the flat case, in agreement with earlier numerical simulations [110], for the circular case $\bar{\lambda}$ was found to be $1/3$. Kallabis and Krug [110] conjectured that the relation obtained for the flat linear growth equations (such as the EW equation), $\bar{\lambda} = \beta + d/z$ (here $d = 1$), also holds in nonlinear growth such as the KPZ class. However, the experimental results for the circular case suggest a modification of the conjecture as follows³⁴ [21]:

$$\bar{\lambda} = \begin{cases} \beta + d/z & (\text{flat subclass}), \\ \beta & (\text{circular subclass}). \end{cases} \quad (86)$$

Moreover, the exponent $\bar{\lambda} = 1/3$ for the circular case suggests that, when translated back into $C_t(t_1, t_2)$ by Eq. (85), $C_t(t_1, t_2)$ remains strictly positive even if $t_2 \rightarrow \infty$. In other words, positive fluctuations tend to remain positive forever and vice versa, suggesting a sort of ergodicity breaking in the circular case. This can be clearly seen by plotting $C_t(t_1, t_2)/C_t(t_1, t_1)$ against $(\Delta t/t_1)^{-2/3}$ with $\Delta t \equiv t_2 - t_1$ [104] (Fig. 16(c)): here, while the flat data go to 0 as $t_2 \rightarrow \infty$ linearly in this plot, the circular data clearly indicate a strictly positive asymptotic value. The authors also measured persistence properties of the height fluctuations, or more precisely, the probability $P_{\text{pers}}(t_1, t_2)$ that $\delta h(x, t) = h(x, t) - \langle h(x, t) \rangle$ with fixed x does not change sign between times t_1 and t_2 [21]. The results showed power-law decay in both cases, $P_{\text{pers}}(t_1, t_2) \sim (t_2/t_1)^{-\theta_{\pm}}$ where \pm indicates the sign of the fluctuations, with the following exponent values:

$$\begin{cases} \theta_+ = 1.35(5) \\ \theta_- = 1.85(10) \end{cases} (\text{flat}) \quad \text{and} \quad \begin{cases} \theta_+ = 0.81(2) \\ \theta_- = 0.80(2) \end{cases} (\text{circular}). \quad (87)$$

Here, the numbers in the parentheses indicate the range of error in the last digit(s). The results for the flat case are consistent with earlier numerics [110] and the inequality $\theta_+ \neq \theta_-$ was associated with the KPZ nonlinear term³⁵ $(\lambda/2)(\nabla h)^2$. In contrast, this asymmetry seems to vanish in the circular case; this remains theoretically unexplained so far. Moreover, since the mean persistence time, i.e., mean time needed for the fluctuations to change the sign, is given

³⁴ For the circular case, the circumference (or equivalently the effective system size) grows with t , faster than the correlation length does, $\xi(t) \sim t^{1/2}$. One can therefore argue that the fluctuations at different spatial positions do not influence the fluctuation at a given point in later times, asymptotically. This is an intuitive reason why, in Eq. (86), the term d/z is not expected for the circular case.

³⁵ Therefore, the values of θ_+ and θ_- are exchanged if $\lambda < 0$ [110].

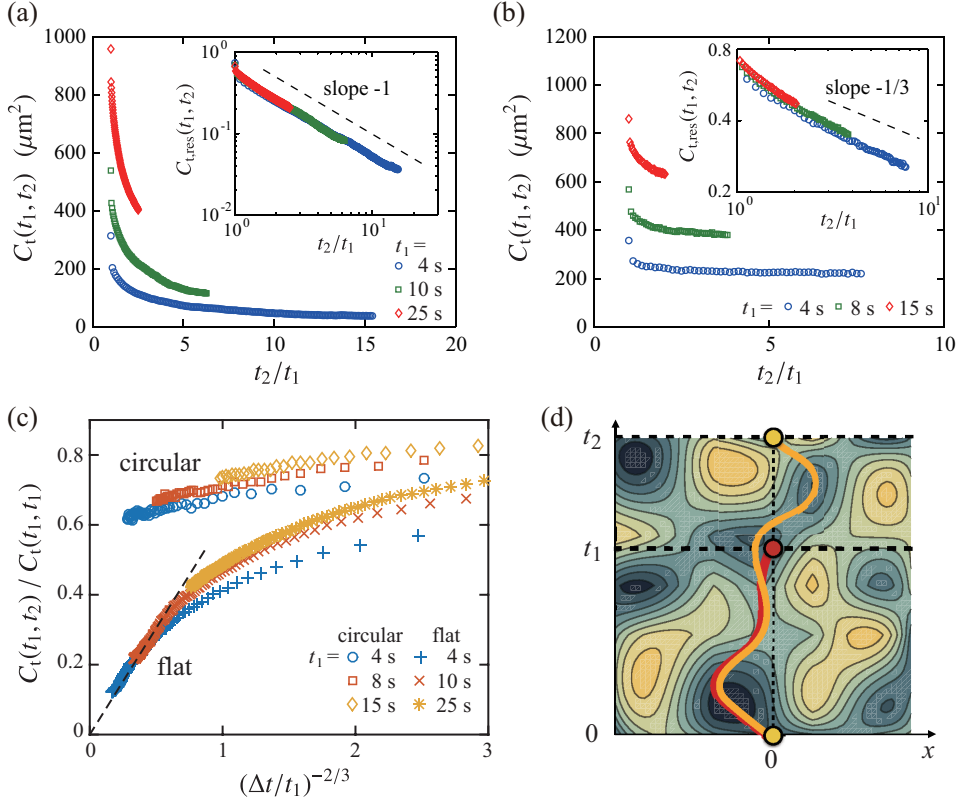


Figure 16: Experimental results of the temporal correlation function [21, 104]. (a,b) Two-time correlation function $C_t(t_1, t_2)$ against t_2/t_1 for the flat (a) and circular (b) interfaces. The insets show the rescaled function $C_{t, \text{res}}(t_1, t_2)$ [21]. (c) Ratio of the two-time correlation function, $C_t(t_1, t_2)/C_t(t_1, t_1)$, against $(\Delta t/t_1)^{-2/3}$ with $\Delta t \equiv t_2 - t_1$. The data for the circular interfaces clearly show that $C_t(t_1, t_2)$ remain strictly positive in the limit $t_2 \rightarrow \infty$. Dashed line is a guide for the eyes. (d) Sketch of the two-time problem in terms of the directed polymer under random potential [104]. Reprints with permission from [21] (a,b) and from [104] (d) with some adaptations.

by $\int P_{\text{pers}}(t_1, t_2) dt_2$, $\theta_{\pm} < 1$ for the circular case implies that it diverges, hence ergodicity breaking in this case.

Recently, theoretical approaches have also become capable of dealing with some two-time properties. Ferrari and Spohn [102] considered TASEP and derived the exponent $\bar{\lambda}$ for the circular, flat, and stationary subclasses. The exponents were indeed $\bar{\lambda} = 1/3$ and 1 for the circular and flat cases, respectively, accounting for the experimental observations. They also showed that the two-time correlation for the stationary subclass, when appropriately rescaled, coincides with that of the fractional Brownian motion with Hurst exponent 1/3 [102]; specifically,

$$F_t(\tau) \sim \langle \chi_0^2 \rangle_c \frac{\tau^{-1/3}}{2} \left[1 + \tau^{2/3} - (\tau - 1)^{2/3} \right] \quad (\text{stationary subclass}), \quad (88)$$

even though the process $\chi(x, t)$ in time is *not* the fractional Brownian motion, because its one-time distribution is not Gaussian but the Baik-Rains distribution. Furthermore, very recently, even analytic expressions of the two-time joint distribution for the circular case were obtained by different authors [101, 103–105]. While the formulas in [101, 103] remain difficult to evaluate numerically, de Nardis and Le Doussal [104, 105] found that an easily tractable form can be obtained by the replica Bethe ansatz approach to the Lieb-Liniger model (76), i.e., the KPZ equation. Their derivation was based on a hint that directed polymers in the point-to-point problem tend to overlap near the origin $(x, t) = (0, 0)$ (Fig. 16(d)), more and more if $h(0, t_1)$ is larger, since then the random potential landscape tends to have a deeper path between times 0 and t_1 (recall that $h(0, t) = \log Z(0, t)$ is the (minus) free energy of the directed polymer). This led them to focus on such eigenstates of \hat{H}_{LL} that all particles are bounded during this time period, and successfully obtained an approximate generating function for the two-time fluctuations. The deviation from the

full problem turned out to be superexponentially small, in the order of $O(e^{-\frac{8}{3}h_{\text{res}}(x,t_1)^{3/2}})$. With this generating function, a number of quantities were numerically evaluated, such as the cumulants and the two-time correlation function conditioned for large $h(x, t_1)$, which were found in agreement experimentally and numerically [104]. In particular, their theory accounted for the strictly positive two-time correlation $C_1(t_1, t_2) > 0$ ($t_2 \rightarrow \infty$) in the circular case, in terms of the overlap of directed polymers (Fig. 16(d)).

7.5. Toward stationary subclass and general initial conditions

While the liquid-crystal experiment has successfully identified a number of universal features of the circular and flat subclasses, the stationary subclass remains to be directly identified. However, signatures of the stationary subclass, in particular the Baik-Rains distribution, were found by crossover analysis [111] and by power spectrum of height fluctuations $\delta h(x, t)$ [112]. The crossover toward the Baik-Rains distribution was also identified numerically [111, 113] and theoretically [104, 105].

It is also interesting to explore other possible geometries of interfaces. To this end, Fukai and Takeuchi [74] developed a technique to generate an arbitrary initial condition in this liquid crystal system and studied interfaces growing from a ring of a finite radius, in the inward direction. This is a circular problem with curvature opposite to the usual circular subclass, and interestingly, they found that the statistical properties agreed with those of the *flat* subclass, until the interfaces become too small in circumference and eventually collapse at the center of the ring [74]. From a similar perspective, recently a number of theoretical studies [114–117] have also considered initial conditions more general than the standard ones. It is hoped that such theoretical and experimental studies will lead to deeper understanding of the subclass structure of the KPZ universality class.

8. Higher dimensions

In Secs.5-7 we have essentially considered the 1D case, but the KPZ class is by no means restricted to the 1D problem. There are no known integrable models that are able to provide exact results for higher dimensions, but numerical and experimental studies have been carried out to investigate the distribution and correlation functions for the 2D case, i.e., surfaces growing in the three-dimensional space. Interestingly, the subclass structure persists in higher dimensions. More specifically, on the basis of numerical results by Halpin-Healy [118, 119] and Oliveira *et al.*[120], there are four canonical subclasses in 2D: sphere (point-to-point), cylinder (point-to-line), flat (point-to-surface), and stationary. Experiments on 2D thin film growth [121–123] indeed found that the experimentally obtained histograms were consistent with the numerical one for the flat 2D subclass.

Theoretically, Kloss *et al.*[124] employed a non-perturbative renormalization group approach and evaluated the two-point correlation function of the stationary subclass, $g_0(\zeta)$. They found, for 1D, a remarkable agreement with the exact result [96]. For 2D and 3D, they provided an estimate of an amplitude ratio R that contains $\langle \chi_0^2 \rangle_c$, i.e., an analogue of the Baik-Rains variance for each dimensionality. Halpin-Healy's 2D numerics showed $R = 0.944 \pm 0.031$ [119, 125] in a remarkable agreement with Kloss *et al.*'s estimate $R = 0.940$ [124]. It remains a great challenge to invent a theoretical framework that can cope with other quantities and subclasses of the higher-dimensional KPZ class.

9. Concluding remarks

The author hopes that these lecture notes provided a convincing overview that our understanding of the KPZ class, in particular for the 1D case, has significantly deepened by recent extensive investigations. As a reminder, Table 1 gives a summary of the three subclasses established in the 1D KPZ class. One might have the impression that most important pieces of work were already done. However, if we recall the history of the equilibrium critical phenomena that is briefly overviewed in Sec. 1, we notice that we are probably still in its mid 20th century or so, by which exact solutions of the 2D Ising model were found and related experimental observations were made. Is there any fundamental theoretical framework, such as counterparts of Wilson's renormalization group and conformal field theory, hidden behind this development for non-equilibrium scale-invariant fluctuations? Can we understand higher-dimensional problems equally well eventually, or at the level comparable to the recent developments on the 3D Ising model? Somewhat optimistically, the author believes that there are fundamental open problems waiting to be found, in the future of studies on the KPZ class and related problems.

Table 1: The three canonical subclasses of the 1D KPZ class.

KPZ subclass	circular	flat	stationary
standard initial condition	narrow-wedge (or point nucleus)	flat	Brownian
	$h(x, 0) = \begin{cases} 0 & (x = 0) \\ -\infty & (x \neq 0) \end{cases}$	$h(x, 0) = 0$	$h(x, 0) = \sqrt{AB}B(x)$
initial condition for ASEP	step (Fig. 10(a))	alternating (Fig. 11(a))	Bernoulli (Fig. 11(b))
exponents	$\alpha = 1/2, \beta = 1/3, z = 3/2$ for all subclasses		
distribution [50]	GUE Tracy-Widom (χ_2)	GOE Tracy-Widom (χ_1)	Baik-Rains (χ_0)
$(\langle \chi_i \rangle, \langle \chi_i^2 \rangle_c, \text{Sk}(\chi_i), \text{Ku}(\chi_i))^a$	(-1.77, 0.813, 0.224, 0.093)	(-0.760, 0.638, 0.293, 0.165)	(0, 1.15, 0.359, 0.289)
spatial process [93]	Airy ₂ process	Airy ₁ process	Airy _{stat} process ^b
(its 2-pt correlation $g_i(\zeta)$)	(power-law decay)	(superexponential decay)	(superexponential decay)
two-time correlation [21, 102]	$F_1(\tau) \sim \tau^{-1/3}$	$F_1(\tau) \sim \tau^{-1}$	$F_1(\tau) \sim \tau^{-1/3}$
persistence exponents ^c	(ergodicity breaking)	(ergodicity breaking)	(ergodicity breaking)
	$\theta_+ \approx 1.35, \theta_- \approx 1.85$ [21]	$\theta_{\pm} \approx 0.80$ [21]	$\theta_{\pm} = 1 - \beta = 2/3$ [110, 126]

^a $\langle \chi_i^n \rangle_c$ denotes the n th-order cumulant of χ_i , $\text{Sk}(\chi_i) \equiv \langle \chi_i^3 \rangle_c / \langle \chi_i^2 \rangle_c^{3/2}$ and $\text{Ku}(\chi_i) \equiv \langle \chi_i^4 \rangle_c / \langle \chi_i^2 \rangle_c^2$. The values are cited from [50], in which more precise values are given.

^b Note the different definition of the spatial process, Eq. (79).

^c The values of θ_+ and θ_- are shown in the case of $\lambda > 0$. They are exchanged otherwise [110].

Acknowledgments

The author is indebted to enlightening discussions with many theoreticians and mathematicians, in particular P. L. Ferrari, P. Grassberger, T. Halpin-Healy, P. Le Doussal, M. Prähofer, T. Sasamoto, G. Schehr, and H. Spohn, to learn the theoretical contents described in these lecture notes. Among others, a series of lectures delivered by T. Sasamoto were important for the author to prepare many parts of the manuscript. Of course, should any mistake be found in these lecture notes, it would be entirely the fault of the author. The author acknowledges the theoretical curves of the Tracy-Widom distributions [Fig. 14(c)] provided by M. Prähofer [61], those of the Airy₁ and Airy₂ two-point correlation functions [Fig. 15] by F. Bornemann [62], permissions of figure reprints by M. A. C. Huergo [Fig. 1(a)], by P. Yunker [Fig. 1(b)], and by J. De Nardis and P. Le Doussal [Fig. 16(d)], and useful comments on the manuscript by T. Halpin-Healy. Finally, the author appreciates financial support by KAKENHI from Japan Society for the Promotion of Science (No. JP25103004, JP16H04033, JP16K13846), the National Science Foundation under Grant No. NSF PHY11-25915, and 2016 Tokyo Tech Challenging Research Award.

References

- [1] H. Nishimori, G. Ortiz, Elements of Phase Transitions and Critical Phenomena, 1st Edition, Oxford Graduate Texts, Oxford Univ. Press, New York, 2011.
- [2] P. Heller, Experimental investigations of critical phenomena, Rep. Prog. Phys. 30 (1967) 731.
- [3] T. Andrews, The Bakerian Lecture: On the continuity of the gaseous and liquid states of matter, Phil. Trans. R. Soc. London 159 (1869) 575–590.
- [4] R. J. Baxter, Exactly Solved Models in Statistical Mechanics, Academic Press, London, 1982.
- [5] L. Onsager, Crystal statistics. I. a two-dimensional model with an order-disorder transition, Phys. Rev. 65 (1944) 117–149.
- [6] B. Kaufman, Crystal statistics. II. partition function evaluated by spinor analysis, Phys. Rev. 76 (1949) 1232–1243.
- [7] Y. Nambu, A note on the eigenvalue problem in crystal statistics, Prog. Theor. Phys. 5 (1950) 1–13.
- [8] K. G. Wilson, The renormalization group: Critical phenomena and the Kondo problem, Rev. Mod. Phys. 47 (1975) 773–840.
- [9] M. Henkel, Conformal Invariance and Critical Phenomena, Springer, Berlin, Heidelberg, New York, 1999.
- [10] S. El-Showk, M. Paulos, D. Poland, S. Rychkov, D. Simmons-Duffin, A. Vichi, Solving the 3d Ising model with the conformal bootstrap II. c-minimization and precise critical exponents, J. Stat. Phys. 157 (2014) 869–914.
- [11] M. Kardar, G. Parisi, Y.-C. Zhang, Dynamic scaling of growing interfaces, Phys. Rev. Lett. 56 (1986) 889–892.
- [12] A.-L. Barabási, H. E. Stanley, Fractal Concepts in Surface Growth, Cambridge Univ. Press, Cambridge, 1995.
- [13] T. Halpin-Healy, Y.-C. Zhang, Kinetic roughening phenomena, stochastic growth, directed polymers and all that. aspects of multidisciplinary statistical mechanics, Phys. Rep. 254 (1995) 215–414.
- [14] T. Kriecherbauer, J. Krug, A pedestrian's view on interacting particle systems, KPZ universality and random matrices, J. Phys. A 43 (2010) 403001.
- [15] I. Corwin, The Kardar-Parisi-Zhang equation and universality class, Random Matrices Theory Appl. 1 (2012) 1130001.

- [16] T. Halpin-Healy, K. A. Takeuchi, A KPZ cocktail - shaken, not stirred...: Toasting 30 years of kinetically roughened surfaces, *J. Stat. Phys.* 160 (2015) 794–814.
- [17] T. Sasamoto, The 1d Kardar-Parisi-Zhang equation: Height distribution and universality, *Prog. Theor. Exp. Phys.* 2016 (2016) 022A01.
- [18] J. Quastel, H. Spohn, The one-dimensional KPZ equation and its universality class, *J. Stat. Phys.* 160 (2015) 965–984.
- [19] K. A. Takeuchi, M. Sano, Universal fluctuations of growing interfaces: Evidence in turbulent liquid crystals, *Phys. Rev. Lett.* 104 (2010) 230601.
- [20] K. A. Takeuchi, M. Sano, T. Sasamoto, H. Spohn, Growing interfaces uncover universal fluctuations behind scale invariance, *Scientific Reports* 1 (2011) 34.
- [21] K. A. Takeuchi, M. Sano, Evidence for geometry-dependent universal fluctuations of the Kardar-Parisi-Zhang interfaces in liquid-crystal turbulence, *J. Stat. Phys.* 147 (2012) 853–890.
- [22] J. S. Rowlinson, B. Widom, *Molecular Theory of Capillarity*, Oxford Univ. Press, Oxford, 1989.
- [23] D. G. A. L. Aarts, M. Schmidt, H. N. W. Lekkerkerker, Direct visual observation of thermal capillary waves, *Science* 304 (2004) 847–850.
- [24] M. A. C. Huelgo, M. A. Pasquale, P. H. González, A. E. Bolzán, A. J. Arvia, Growth dynamics of cancer cell colonies and their comparison with noncancerous cells, *Phys. Rev. E* 85 (2012) 011918.
- [25] M. A. C. Huelgo, M. A. Pasquale, A. E. Bolzán, A. J. Arvia, P. H. González, Morphology and dynamic scaling analysis of cell colonies with linear growth fronts, *Phys. Rev. E* 82 (2010) 031903.
- [26] M. A. C. Huelgo, M. A. Pasquale, P. H. González, A. E. Bolzán, A. J. Arvia, Dynamics and morphology characteristics of cell colonies with radially spreading growth fronts, *Phys. Rev. E* 84 (2011) 021917.
- [27] P. J. Yunker, T. Still, M. A. Lohr, A. G. Yodh, Suppression of the coffee-ring effect by shape-dependent capillary interactions, *Nature* 476 (2011) 308–311.
- [28] P. J. Yunker, M. A. Lohr, T. Still, A. Borodin, D. J. Durian, A. G. Yodh, Effects of particle shape on growth dynamics at edges of evaporating drops of colloidal suspensions, *Phys. Rev. Lett.* 110 (2013) 035501.
- [29] K. A. Takeuchi, Experimental approaches to universal out-of-equilibrium scaling laws: turbulent liquid crystal and other developments, *J. Stat. Mech.* 2014 (2014) P01006.
- [30] A. Maritan, F. Toigo, J. Koplik, J. R. Banavar, Dynamics of growing interfaces, *Phys. Rev. Lett.* 69 (1992) 3193–3195.
- [31] M. Marsili, Y.-C. Zhang, Overhangs in interface growth and ground-state paths, *Phys. Rev. E* 57 (1998) 4814–4816.
- [32] J. Rodríguez-Laguna, S. N. Santalla, R. Cuerno, Intrinsic geometry approach to surface kinetic roughening, *J. Stat. Mech.* 2011 (2011) P05032.
- [33] P. Grassberger, Universality of critically pinned interfaces in 2-dimensional isotropic random media (2017). [arXiv:1711.02904](https://arxiv.org/abs/1711.02904).
- [34] C. W. Gardiner, *Handbook of Stochastic Methods for Physics, Chemistry and the Natural Sciences*, 3rd Edition, Springer Series in Synergetics, Springer, Berlin, 2004.
- [35] A. Pagnani, G. Parisi, Numerical estimate of the Kardar-Parisi-Zhang universality class in (2+1) dimensions, *Phys. Rev. E* 92 (2015) 010101.
- [36] J. Kelling, G. Ódor, S. Gemming, Dynamical universality classes of simple growth and lattice gas models (2017). [arXiv:1701.03638](https://arxiv.org/abs/1701.03638).
- [37] H. Hinrichsen, Non-equilibrium critical phenomena and phase transitions into absorbing states, *Adv. Phys.* 49 (2000) 815–958.
- [38] H. Ji, M. O. Robbins, Percolative, self-affine, and faceted domain growth in random three-dimensional magnets, *Phys. Rev. B* 46 (1992) 14519–14527.
- [39] G. Bizhani, M. Paczuski, P. Grassberger, Discontinuous percolation transitions in epidemic processes, surface depinning in random media, and hamiltonian random graphs, *Phys. Rev. E* 86 (2012) 011128.
- [40] H.-K. Janssen, M. Müller, O. Stenull, Generalized epidemic process and tricritical dynamic percolation, *Phys. Rev. E* 70 (2004) 026114.
- [41] D. Forster, D. R. Nelson, M. J. Stephen, Large-distance and long-time properties of a randomly stirred fluid, *Phys. Rev. A* 16 (1977) 732–749.
- [42] U. Deker, F. Haake, Fluctuation-dissipation theorems for classical processes, *Phys. Rev. A* 11 (1975) 2043–2056.
- [43] L. Bertini, G. Giacomin, Stochastic Burgers and KPZ equations from particle systems, *Commun. Math. Phys.* 183 (1997) 571–607.
- [44] T. Sasamoto, H. Spohn, One-dimensional Kardar-Parisi-Zhang equation: An exact solution and its universality, *Phys. Rev. Lett.* 104 (2010) 230602.
- [45] T. Sasamoto, H. Spohn, Exact height distributions for the KPZ equation with narrow wedge initial condition, *Nucl. Phys. B* 834 (2010) 523–542.
- [46] G. Amir, I. Corwin, J. Quastel, Probability distribution of the free energy of the continuum directed random polymer in 1+1 dimensions, *Commun. Pure Appl. Math.* 64 (2011) 466–537.
- [47] M. Hairer, Solving the KPZ equation, *Ann. Math.* 178 (2013) 559–664.
- [48] M. Hairer, A theory of regularity structures, *Invent. Math.* 198 (2014) 269–504.
- [49] K. Johansson, Shape fluctuations and random matrices, *Commun. Math. Phys.* 209 (2000) 437–476.
- [50] M. Prähofer, H. Spohn, Universal distributions for growth processes in 1 + 1 dimensions and random matrices, *Phys. Rev. Lett.* 84 (2000) 4882–4885.
- [51] P. Calabrese, P. Le Doussal, A. Rosso, Free-energy distribution of the directed polymer at high temperature, *Europhys. Lett.* 90 (2010) 20002.
- [52] V. Dotsenko, Bethe ansatz derivation of the Tracy-Widom distribution for one-dimensional directed polymers, *Europhys. Lett.* 90 (2010) 20003.
- [53] P. Calabrese, P. Le Doussal, Exact solution for the Kardar-Parisi-Zhang equation with flat initial conditions, *Phys. Rev. Lett.* 106 (2011) 250603.
- [54] T. Imamura, T. Sasamoto, Exact solution for the stationary Kardar-Parisi-Zhang equation, *Phys. Rev. Lett.* 108 (2012) 190603.
- [55] A. Borodin, I. Corwin, P. Ferrari, B. Vető, Height fluctuations for the stationary KPZ equation, *Math. Phys. Anal. Geom.* 18 (2015) 20.
- [56] J. Baik, P. Deift, K. Johansson, On the distribution of the length of the longest increasing subsequence of random permutations, *J. Am. Math. Soc.* 12 (1999) 1119–1178.
- [57] M. L. Mehta, *Random Matrices*, 3rd Edition, Vol. 142 of Pure and Applied Mathematics, Elsevier, San Diego, 2004.

- [58] G. W. Anderson, A. Guionnet, O. Zeitouni, *An Introduction to Random Matrices*, Cambridge Studies in Advanced Mathematics, Cambridge Univ. Press, Cambridge, 2009.
- [59] C. A. Tracy, H. Widom, Level-spacing distributions and the Airy kernel, *Commun. Math. Phys.* 159 (1994) 151–174.
- [60] C. A. Tracy, H. Widom, On orthogonal and symplectic matrix ensembles, *Commun. Math. Phys.* 177 (1996) 727–754.
- [61] A numerical table of the GUE and GOE Tracy-Widom distribution, as well as the Baik-Rains distribution, can be downloaded by courtesy of M. Prähofer and H. Spohn from <https://www-m5.ma.tum.de/KPZ>.
- [62] F. Bornemann, On the numerical evaluation of Fredholm determinants, *Math. Comput.* 79 (2010) 871–915.
- [63] R. M. Conte, M. Musette, *The Painlevé Handbook*, Springer, Dordrecht, 2008.
- [64] S. N. Majumdar, G. Schehr, Top eigenvalue of a random matrix: large deviations and third order phase transition, *J. Stat. Mech.* 2014 (2014) P01012.
- [65] J. Baik, E. M. Rains, Symmetrized random permutations, in: P. Bleher, A. Its (Eds.), *Random Matrix Models and Their Applications*, Vol. 40 of MSRI Publications, Cambridge Univ. Press, Cambridge, 2001, pp. 1–19.
- [66] K. Johansson, Discrete polynuclear growth and determinantal processes, *Commun. Math. Phys.* 242 (2003) 277–329.
- [67] P. J. Forrester, S. N. Majumdar, G. Schehr, Non-intersecting Brownian walkers and Yang-Mills theory on the sphere, *Nucl. Phys. B* 844 (2011) 500–526.
- [68] I. Corwin, J. Quastel, D. Remenik, Continuum statistics of the Airy₂ process, *Commun. Math. Phys.* 317 (2013) 347–362.
- [69] J. Baik, E. M. Rains, Limiting distributions for a polynuclear growth model with external sources, *J. Stat. Phys.* 100 (2000) 523–541.
- [70] J. Krug, P. Meakin, Universal finite-size effects in the rate of growth processes, *J. Phys. A* 23 (1990) L987–L994.
- [71] J. Krug, P. Meakin, T. Halpin-Healy, Amplitude universality for driven interfaces and directed polymers in random media, *Phys. Rev. A* 45 (1992) 638–653.
- [72] P. L. Ferrari, R. Frings, Finite time corrections in KPZ growth models, *J. Stat. Phys.* 144 (2011) 1123–1150.
- [73] S. G. Alves, T. J. Oliveira, S. C. Ferreira, Non-universal parameters, corrections and universality in Kardar-Parisi-Zhang growth, *J. Stat. Mech.* 2013 (2013) P05007.
- [74] Y. T. Fukai, K. A. Takeuchi, Kardar-Parisi-Zhang interfaces with inward growth, *Phys. Rev. Lett.* 119 (2017) 030602.
- [75] B. Derrida, An exactly soluble non-equilibrium system: The asymmetric simple exclusion process, *Phys. Rep.* 301 (1998) 65–83.
- [76] O. Golinelli, K. Mallick, The asymmetric simple exclusion process: an integrable model for non-equilibrium statistical mechanics, *J. Phys. A* 39 (2006) 12679–12705.
- [77] P. L. Ferrari, Slow decorrelations in Kardar-Parisi-Zhang growth, *J. Stat. Mech.* 2008 (2008) P07022.
- [78] I. Corwin, P. L. Ferrari, S. Péché, Universality of slow decorrelation in KPZ growth, *Ann. Inst. H. Poincaré B Probab. Statist.* 48 (2012) 134–150.
- [79] A. Borodin, P. L. Ferrari, M. Prähofer, T. Sasamoto, Fluctuation properties of the TASEP with periodic initial configuration, *J. Stat. Phys.* 129 (2007) 1055–1080.
- [80] P. L. Ferrari, H. Spohn, Scaling limit for the space-time covariance of the stationary totally asymmetric simple exclusion process, *Commun. Math. Phys.* 265 (2006) 1–44.
- [81] C. A. Tracy, H. Widom, Asymptotics in ASEP with step initial condition, *Commun. Math. Phys.* 290 (2009) 129–154.
- [82] A. Aggarwal, Current fluctuations of the stationary ASEP and six-vertex model (2016). [arXiv:1608.04726](https://arxiv.org/abs/1608.04726).
- [83] A. Aggarwal, Convergence of the stochastic six-vertex model to the ASEP, *Math. Phys. Anal. Geom.* 20 (2016) 3.
- [84] T. Thiery, P. Le Doussal, On integrable directed polymer models on the square lattice, *J. Phys. A* 48 (2015) 465001.
- [85] E. Medina, M. Kardar, Quantum interference effects for strongly localized electrons, *Phys. Rev. B* 46 (1992) 9984–10006.
- [86] A. M. Somoza, M. Ortuño, J. Prior, Universal distribution functions in two-dimensional localized systems, *Phys. Rev. Lett.* 99 (2007) 116602.
- [87] A. M. Somoza, P. Le Doussal, M. Ortuño, Unbinding transition in semi-infinite two-dimensional localized systems, *Phys. Rev. B* 91 (2015) 155413.
- [88] F. Franchini, *An Introduction to Integrable Techniques for One-Dimensional Quantum Systems*, Vol. 940 of Lecture Notes in Physics, Springer, 2017, preprint [arXiv:1609.02100](https://arxiv.org/abs/1609.02100).
- [89] S. N. Majumdar, Brownian functionals in physics and computer science, *Curr. Sci.* 89 (2005) 2076, preprint [arXiv:cond-mat/0510064](https://arxiv.org/abs/cond-mat/0510064).
- [90] E. H. Lieb, W. Liniger, Exact analysis of an interacting Bose gas. I. the general solution and the ground state, *Phys. Rev.* 130 (1963) 1605–1616.
- [91] N. Fabbri, M. Panfil, D. Clément, L. Fallani, M. Inguscio, C. Fort, J.-S. Caux, Dynamical structure factor of one-dimensional Bose gases: Experimental signatures of beyond-Luttinger-liquid physics, *Phys. Rev. A* 91 (2015) 043617.
- [92] F. Meinert, M. Panfil, M. J. Mark, K. Lauber, J.-S. Caux, H.-C. Nägerl, Probing the excitations of a Lieb-Liniger gas from weak to strong coupling, *Phys. Rev. Lett.* 115 (2015) 085301.
- [93] J. Quastel, D. Remenik, Airy processes and variational problems (2013). [arXiv:1301.0750](https://arxiv.org/abs/1301.0750).
- [94] M. Prähofer, H. Spohn, Scale invariance of the PNG droplet and the Airy process, *J. Stat. Phys.* 108 (2002) 1071–1106.
- [95] T. Sasamoto, Spatial correlations of the 1D KPZ surface on a flat substrate, *J. Phys. A* 38 (2005) L549–L556.
- [96] M. Prähofer, H. Spohn, Exact scaling functions for one-dimensional stationary KPZ growth, *J. Stat. Phys.* 115 (2004) 255–279.
- [97] J. Baik, P. L. Ferrari, S. Péché, Limit process of stationary TASEP near the characteristic line, *Commun. Pure Appl. Math.* 63 (2010) 1017–1070.
- [98] F. Bornemann, P. L. Ferrari, M. Prähofer, The Airy₁ process is not the limit of the largest eigenvalue in GOE matrix diffusion, *J. Stat. Phys.* 133 (2008) 405–415.
- [99] M. Adler, P. van Moerbeke, PDEs for the joint distributions of the Dyson, Airy and sine processes, *Ann. Probab.* 33 (2005) 1326–1361.
- [100] Private communications with P. L. Ferrari (2017).
- [101] V. Dotsenko, Two-time free energy distribution function in (1+1) directed polymers, *J. Stat. Mech.* 2013 (2013) P06017.
- [102] P. L. Ferrari, H. Spohn, On time correlations for KPZ growth in one dimension, *SIGMA* 12 (2016) 074.
- [103] K. Johansson, Two time distribution in Brownian directed percolation, *Commun. Math. Phys.* 351 (2017) 441–492.

- [104] J. De Nardis, P. Le Doussal, K. A. Takeuchi, Memory and universality in interface growth, *Phys. Rev. Lett.* 118 (2017) 125701.
- [105] J. de Nardis, P. Le Doussal, Tail of the two-time height distribution for KPZ growth in one dimension, *J. Stat. Mech.* 2017 (2017) 053212.
- [106] J.-i. Wakita, H. Itoh, T. Matsuyama, M. Matsushita, Self-affinity for the growing interface of bacterial colonies, *J. Phys. Soc. Jpn.* 66 (1997) 67–72.
- [107] J. Maunuksele, M. Mylly, O.-P. Kähkönen, J. Timonen, N. Provatas, M. J. Alava, T. Ala-Nissila, Kinetic roughening in slow combustion of paper, *Phys. Rev. Lett.* 79 (1997) 1515–1518.
- [108] M. Mylly, J. Maunuksele, M. Alava, T. Ala-Nissila, J. Merikoski, J. Timonen, Kinetic roughening in slow combustion of paper, *Phys. Rev. E* 64 (2001) 036101.
- [109] P. G. de Gennes, J. Prost, *The Physics of Liquid Crystals*, 2nd Edition, Vol. 83 of International Series of Monographs on Physics, Oxford Univ. Press, New York, 1995.
- [110] H. Kallabis, J. Krug, Persistence of Kardar-Parisi-Zhang interfaces, *Europhys. Lett.* 45 (1999) 20–25.
- [111] K. A. Takeuchi, Crossover from growing to stationary interfaces in the Kardar-Parisi-Zhang class, *Phys. Rev. Lett.* 110 (2013) 210604.
- [112] K. A. Takeuchi, $1/f^\alpha$ power spectrum in the Kardar-Parisi-Zhang universality class, *J. Phys. A* 50 (2017) 264006.
- [113] T. Halpin-Healy, Y. Lin, Universal aspects of curved, flat, and stationary-state Kardar-Parisi-Zhang statistics, *Phys. Rev. E* 89 (2014) 010103.
- [114] J. Quastel, D. Remenik, How flat is flat in random interface growth? (2016). [arXiv:1606.09228](https://arxiv.org/abs/1606.09228).
- [115] S. Chhita, P. Ferrari, H. Spohn, Limit distributions for KPZ growth models with spatially homogeneous random initial conditions (2016). [arXiv:1611.06690](https://arxiv.org/abs/1611.06690).
- [116] K. Matetski, J. Quastel, D. Remenik, The KPZ fixed point (2017). [arXiv:1701.00018](https://arxiv.org/abs/1701.00018).
- [117] P. Le Doussal, Crossover between various initial conditions in KPZ growth: flat to stationary (2017). [arXiv:1701.02305](https://arxiv.org/abs/1701.02305).
- [118] T. Halpin-Healy, (2+1)-dimensional directed polymer in a random medium: Scaling phenomena and universal distributions, *Phys. Rev. Lett.* 109 (2012) 170602.
- [119] T. Halpin-Healy, Extremal paths, the stochastic heat equation, and the three-dimensional Kardar-Parisi-Zhang universality class, *Phys. Rev. E* 88 (2013) 042118.
- [120] T. J. Oliveira, S. G. Alves, S. C. Ferreira, Kardar-Parisi-Zhang universality class in (2+1) dimensions: Universal geometry-dependent distributions and finite-time corrections, *Phys. Rev. E* 87 (2013) 040102.
- [121] T. Halpin-Healy, G. Palasantzas, Universal correlators and distributions as experimental signatures of (2+1)-dimensional Kardar-Parisi-Zhang growth, *Europhys. Lett.* 105 (2014) 50001.
- [122] R. A. L. Almeida, S. O. Ferreira, T. J. Oliveira, F. D. A. A. Reis, Universal fluctuations in the growth of semiconductor thin films, *Phys. Rev. B* 89 (2014) 045309.
- [123] R. A. L. Almeida, S. O. Ferreira, I. R. B. Ribeiro, T. J. Oliveira, Temperature effect on (2+1) experimental Kardar-Parisi-Zhang growth, *Europhys. Lett.* 109 (2015) 46003.
- [124] T. Kloss, L. Canet, N. Wschebor, Nonperturbative renormalization group for the stationary Kardar-Parisi-Zhang equation: Scaling functions and amplitude ratios in 1+1, 2+1, and 3+1 dimensions, *Phys. Rev. E* 86 (2012) 051124.
- [125] T. Halpin-Healy, Erratum: Extremal paths, the stochastic heat equation, and the three-dimensional Kardar-Parisi-Zhang universality class [*Phys. Rev. E* 88, 042118 (2013)], *Phys. Rev. E* 88 (2013) 069903.
- [126] J. Krug, H. Kallabis, S. N. Majumdar, S. J. Cornell, A. J. Bray, C. Sire, Persistence exponents for fluctuating interfaces, *Phys. Rev. E* 56 (1997) 2702–2712.